STITCH WELD EFFECT ON SOLAR COLLECTOR EFFICIENCY FACTOR

by

Andy K. LO

B.Sc., Queen's University at Kingston, 1983

A THESIS SUBMITTED IN PARTIAL FULFILMENT OF THE REQUIREMENTS FOR THE DEGREE OF MASTER OF APPLIED SCIENCE

in

FACULTY OF GRADUATE STUDIES

DEPARTMENT OF MECHANICAL ENGINEERING

We accept this thesis as conforming to the required standard

UNIVERSITY OF BRITISH COLUMBIA

September, 1985

In presenting this thesis in partial fulfilment of the requirements for an advanced degree at the University of British Columbia, I agree that the Library shall make it freely available for reference and study. I further agree that permission for extensive copying of this thesis for scholarly purposes may be granted by the head of my department or by his or her representatives. It is understood that copying or publication of this thesis for financial gain shall not be allowed without my written permission.

Department of MECHANICAL ENGINEERING

The University of British Columbia
1956 Main Mall
Vancouver, Canada
V6T 1Y3

Date October 9, 1985

DE-6(3/81)

ABSTRACT

The thermal effects of stitch welding the coolant conduits of a water-cooled flat plate solar collector to its absorber plate have been studied. A physical model of the heat transfer process from the plate to the fluid flowing inside the tube has been presented. The heat transfer coefficient based on the difference between bond temperature and fluid bulk mean temperature is an important factor in determining the collector efficiency factor F'.

The upper and lower limits of the actual value of F' have been predicted by considering two extreme boundary conditions to which the fluid is subjected. For a thick and conductive tube wall, F' does not depend on spot size and spot spacing, and tends to an upper limit of 0.883. For a thin and non-conductive tube wall, the boundary condition comprises of a series of step changes in both the axial and circumferential directions of the heat flux. In this case, the heat transfer coefficient and hence F' approach their lower limits which are determined by the welding spot configuration. It was also found that F' increases with the following parameters: the spot angle; the percentage of tube length being welded; and the number of spots among which the welding is being distributed. Furthermore, the temperature distribution inside the fluid has also been computed for this case.

Table of Contents

LIST OF TABLES

LIST OF FIGURES

LIST OF SYMBOLS

A	cross sectional area, [m^2]
a	tube inner radius, [m]
B	wall conductance parameter (= $k_w\gamma/ka$)
b	bond width, [m]
C_b	bond conductance, [W/m °C]
c_p	specific heat capacity of fluid, [J/kg°C]
D	tube inner diameter (=2a), [m]
F	fin efficiency parameter
F'	collector efficiency factor
$\overrightarrow{g}$	vectorial body forces, [N]
h	convective heat transfer coefficient, [$W/m^2°C$]
I	internal energy per unit mass, [J/kg]
k	thermal conductivity of fluid, [W/m°C]
k_s	thermal conductivity of fin material, [W/m°C]
k_w	thermal conductivity of tube wall, [W/m°C]
L	tube length, [m]
m	$\sqrt{(U_L/k_s\delta)}$, a factor appearing in the fin efficiency F.
$\dot{m}$	fluid mass flow rate, [kg/s]
M_r	maximum radial node no.
M_x	maximum axial node no.
M_ϕ	maximum circumferential node no.
N	total no. of welding spots along a tube
N_r	radial node no.

N_x	axial node no.
N_ϕ	circumferential node no.
Nu	local Nusselt no.
Nu_b	Nusselt no. based on bond temperature
Nu_{bm}	mean Nusselt no. based on bond temperature
Nu_p	peripheral average Nusselt no.
Nu_m	mean Nusselt no. based on Nu_p
p	pressure, [N/m^2]
Pe	Peclet No. (=Re.Pr)
q	wall heat flux into fluid, [W/m^2]
$\bar{q}$	peripheral average wall heat flux, [W/m^2]
q_u	useful energy gain per unit length per tube in the flow direction, [W/m]
Q_{sol}	incident solar heat flux, [W/m^2]
R	radial co-ordinate, [m]
r	dimensionless radial co-ordinate (= R/a)
R_w	wall resistance coefficient (= $k\gamma/k_w D$)
Re	Reynolds no.
S	stress tensor
T	temperature, [°C]
T_{in}	fluid inlet temperature, [°C]
T_m	fluid bulk mean temperature, [°C]
T_w	inner wall temperature of tube, [°C]
T_{wm}	peripheral average wall temperature, [°C]

t	dimensionless temperature (= $k(T-T_{in})/\bar{q}a$)
t_{in}, t_m, t_w, t_{wm}	dimensionless counterparts of T_{in}, T_m, T_w, T_{wm}
U	peak flow speed (=$2\bar{u}$ for parabolic profile)
u	axial component of flow velocity, [m/s]
$\bar{u}$	mean flow speed, [m/s]
U_L	collector overall heat transfer coefficient, [W/m²°C]
$\overline{V}$	fluid velocity [m/s]
W	distance between tubes, [m]
w	welded percentage of tube length
X	axial co-ordinate, [m]
x	dimensionless axial co-ordinate (= X/a.Re.Pr)
X_1, X_s	spot length and spot spacing, [m]
x_1, x_s	X_1/a.Re.Pr and X_s/a.Re.Pr
a	thermal diffusivity (= $k/\rho c_p$),[m²/s]
γ	tube wall thickness, [m]
δ	fin thickness, [m]
ϕ	peripheral co-ordinate, [radians]
ϕ_o	half-spot angle [radians]
μ	dynamic viscosity, [kg/m.s]
ν	kinematic viscosity, [m²/s]
τ	time, [s]
θ	dimensionless temp. (= $(T - T_w)/(T_{in} - T_w)$)

ACKNOWLEDGEMENTS

The author considers himself fortunate to have had Dr. E.G. Hauptmann and Dr. M. Iqbal as his supervisors throughout this study. Their guidance and assistance have been crucial towards the completion of this work.

The University of British Columbia provided this wonderful site of studying and the computing facilities.

Finally, the author wishes to thank his family members, some from half-way across the world, who have given spiritual support and encouragement throughout this work.

1. INTRODUCTION

1.1 GENERAL

Heat transfer phenomena in a water-cooled solar collector include solar radiation, conductive and convective cooling to the ambient, and internal flow forced convective heat transfer. The most common type of solar collector used in building heating and water heating is the flat plate water-cooled type as shown in Figure 1.1. Figure 1.2 shows the manner in which the various modes of heat transfer are involved.

The black, solar energy-absorbing plate has means for transferring the absorbed energy to a fluid, usually through welded tubes in which flowing water carries away the heat being absorbed. Calculating the amount of heat being carried away is the aim of forced convective heat transfer analysis in internal flows. One or two envelopes cover the solar absorber surface. The covers are transparent to incoming solar radiation but opaque to the thermal radiation from the absorber plate, thus reducing convective and radiative losses to the atmosphere. A back insulation is included to reduce conductive losses [1].

Flat plate collectors are almost always stationary and positioned with an orientation optimized for the particular location in question, and for the time of year in which the solar device is intended to operate. Without optical concentration, the flux of incident radiation is, at best,

1100 W/m^2. Both beam and diffuse radiation are being absorbed by the collector, which can be designed for applications requiring energy delivery at moderate temperatures.

The flow of coolant in the welded tube is commonly in the laminar regime. Laminar flow heat transfer is of great technical importance since it occurs in many heating and cooling devices. The heat transfer coefficient between the absorber plate and the cooling water is an important factor in solar collector design since it determines the collector efficiency, and hence the economic value of the installation.

The performance of a solar water heater is directly proportional to its **efficiency factor** F', which represents the ratio of the actual useful energy gain to the useful energy gain that would result if the collector absorbing surface had been at the local fluid temperature. Another interpretation of F' is that it is a measure of the efficiency of the design as a heat exchanger [2]. A cross-section of the plate and tube arrangement is shown in Figure 1.3. The collector efficiency factor is

$$F' = \frac{1/U_L}{W\{\ 1/[U_L(b+(W-b)F)] + 1/C_b + \gamma/(\pi D k_w) + 1/(\pi D h)\}}, \qquad (1.1)$$

where the dimensions are as indicated in Figure 1.3, and the other terms, which appeared in the "LIST OF SYMBOLS", are repeated here :

U_L = overall coefficient of heat transfer from the flat plate to the outside air, including allowance for rear losses,

h = coefficient of heat transfer from the tube wall to the water in the tube,

k_s, k_w = thermal conductivities of the plate and tube materials respectively,

C_b = thermal conductance of the tube-plate bond,

$$F = \frac{\tanh[m(W-b)/2]}{m(W-b)/2} = \text{fin efficiency;}$$

$$m = \sqrt{(U_L/k_s\delta)}.$$

In equation (1.1) the four terms in the right hand denominator can be thought of as the relative resistance to the passage of heat from the plate into the water due to :

(1) conduction of heat along the flat plate towards the tubes,

(2) conduction of heat from the plate to the tube through the tube-plate bond,

(3) conduction throughout the tube wall to the inner surface of the tube,

(4) transfer of heat from the tube inner surface into the water.

The governing equations of fluid flow inside a circular tube, namely, 1) the **continuity** equation, 2) the **momentum** equation, and 3) the **energy** equation, have been well formulated and extensively studied. Although an energy

equation can be written to describe the temperature of the water flowing inside the collector tube, the boundary conditions on the water depend on the configuration of the collector. An important aspect is the fashion in which the tube is welded onto the fin (the absorber plate). A number of common ways of bonding are shown and briefly described in Figures 1.4(i) - (iv). An **ultrasonic spot welding** process is often used for economic reasons. In this case the boundary condition in the axial direction can be considered as a series of step changes (Figure 1.4(iv)).

In conventional studies of convective heat transfer, the mathematical model of the problem includes well defined boundary conditions concerning the temperature or the heat flux. The temperature or the heat flux is clearly specified mathematically at the boundary of the region of interest, which is the inside tube wall in the present case. In reality, because of axial and peripheral heat conduction in the tube material, the flowing water is subject to a boundary condition at the wall which can neither be described in terms of wall temperature nor wall heat flux. The so-called "conjugated problem" deals with this situation by taking into account the conduction in the solid material.

1.2 OBJECTIVE OF THE PRESENT WORK

Although laminar convective heat transfer has been extensively studied for various kinds of boundary conditions, no practical solution is available for flows in

the spot-welded tube as shown in Figure 1.4(iv). The objective of this work is to investigate the effects of the spot and spacing dimensions on the heat transfer coefficient between the tube wall and the fluid. Knowing this coefficient, the consequential effect on collector performance, and in particular the collector efficiency factor can be determined.

The question of spot spacing is of great economic importance since the welding process is slow and consumes energy. By knowing how far apart the spots can be located before the collector efficiency is significantly reduced, an optimum set of spot length and spot spacing can be determined (taking welding costs into account). As a start, however, the heat transfer process from the spot-welded tube to the fluid flowing inside must be understood. This understanding should be in terms of the dimensionless temperature distribution in the fluid, and in terms of the **mean Nusselt number**, which is the dimensionless form of the mean heat transfer coefficient from the circular tube to the fluid.

Obviously, the heat flux into the water is higher through the welding spots than through the rest of the tube. An extreme case exists when the tube wall is vanishingly thin so that peripheral and axial conduction within the wall material is negligible, and the heat flux from the absorber plate enters the water only through the welding spots. At the other extreme, if the tube material is highly conductive

and the wall is thick, conduction within the wall material occurs in all directions and temperature variation in the wall will be reduced. In this case, the water is subject to a boundary of uniform temperature. In reality, however, neither of these conditions prevail.

Analytical solutions to the convective heat transfer process involved in the above extreme cases were sought for various configurations of spots and spacings and checked against numerical solutions. The results of the collector efficiency factor of these extreme models can be used as limits of the realistic situation.

1.3 LITERATURE REVIEW

Internal flow convective heat transfer in various geometries under various boundary conditions has been studied in great detail in the literature. A major review of work in laminar flow forced convection has been done by Shah and London [3], including various duct geometries and boundary conditions. The scope of the present review is restricted to forced convective laminar flow for a Newtonian fluid with constant properties, passing through stationary, straight, non-porous ducts of constant circular cross section. The literature was reviewed under four problem categories :

1. Entry length problems in duct flows;
2. The Graetz problem and its two classical methods of solution;

3. Problems with circumferential variation, with an axially developed or developing thermal profile; and
4. Conjugated problems, where heat conduction in the tube material is taken into consideration.

1.3.1 THE ENTRY LENGTH PROBLEM

In forced convective heat transfer in ducts, fluid flow is often categorized according to its velocity and temperature profile. The temperature and velocity profiles of the fluid begin to develop at the entrance to a tube. The flow is termed **hydrodynamically developed** where the velocity profile is already fully established and does not change as the fluid travels downstream. Similarly, where the heat transfer coefficient is axially invariant the flow is considered to be **thermally developed.** The downstream distances from the entrance required before the flow becomes hydrodynamically and thermally developed are called the hydrodynamic and thermal **entry lengths**, respectively, as illustrated in Figure 1.5.

A thermally and hydrodynamically developing flow is more complicated than a thermally developing but hydrodynamically developed flow. It has been shown [4], however, that if the Prandtl number Pr of the fluid is greater than about 5, the velocity profile development leads the temperature profile development and it is sufficiently accurate to consider the flow at the entrance as hydrodynamically developed, even though there is no

hydrodynamic starting length.

1.3.2 GRAETZ PROBLEM

Graetz [5] in 1883 considered an incompressible fluid with constant physical properties flowing through a circular tube, hydrodynamically fully developed and with a developing thermal profile. The tube is maintained at a constant and uniform temperature. The energy equation is

$$u \frac{\partial T}{\partial X} = \alpha \left(\frac{\partial^2 T}{\partial R^2} + \frac{1}{R} \frac{\partial T}{\partial R} \right) , \qquad (1.2)$$

The boundary conditions are :

For $X \leq 0$, $T = T_{in}$ = constant,

for $X > 0$ at $R = a$, $T = T_w$ = constant,

at $R = 0$, $\partial T/\partial R = 0$.

The physical situation is as shown in Figure 1.6, and is now known as the Graetz problem. A review of earlier work on the Graetz problem has been done by Drew [6]. Brown [7] also provided a comprehensive literature survey for the Graetz problem. The closed form solution to this problem has been obtained primarily by two methods : the Graetz method and the Leveque method.

The Graetz method uses the separation of variables technique and as a result the differential equation (1.2) is reduced to the Sturm-Liouville type. The solution is then obtained in the form of an infinite series expansion of eigenvalues and eigenfunctions. The number of terms required

for a desired accuracy increases sharply as $x = X/(a.Re.Pr)$ approaches zero.

The Graetz solution to the problem, in terms of the temperature distribution, is presented in an infinite series

$$\theta = (T - T_w)/(T_{in} - T_w) = \sum_{n=1}^{\infty} c_n R_n \exp(-\lambda_n^2 x) \ , \qquad (1.3)$$

where R_n are the eigenfunctions in r, λ_n are the eigenvalues, and c_n are constants. Graetz and Nusselt obtained only the first two and three terms, respectively, of the series [3]. Sellars et al. [8] independently determined the first ten eigenvalues and constants, and presented asymptotic formulas for the higher ones.

The Leveque [9] method employs the similarity transformation technique and its solution to the resulting equation is valid only near $x = 0$. It employs the "flat plate" solution as an asymptotic approximation near the point where the step change in temperature occurs. The velocity distribution in the thermal boundary layer was assumed linear and having the same slope as that at the wall with $u = 0$ at wall. The situation is illustrated in Figure 1.7. Leveque obtained the following solution for the circular tube :

$$\theta = (T - T_w)/(T_{in} - T_w) = [1/\Gamma(4/3)] \int_0^{\eta} \exp(-z^3)dz \ , \qquad (1.4)$$

where $\eta = \dfrac{1 - R/a}{(9x/2)^{1/3}}$,

and Γ is the gamma function : $\Gamma(n) = \int_0^\infty (e^{-z} z^{n-1}) dz$.

Mercer [10], Worsoe-Schmidt [11] and Newman [12] have extended the Leveque solution by a perturbation method solving the energy equation (equ 1.2) directly. The corresponding solution is

$$\theta(\xi,\eta) = \sum_{n=0}^{N} \xi^n \theta_n(\eta) \quad , \qquad (1.5)$$

where $\xi = (9x/2)^{1/3}$ for the circlar tube. The first term in this series corresponds to Leveque's solution. This solution is valid for intermediate values of x where both the Graetz and Leveque solutions are not accurate.

Grigull and Tratz [13] solved equation (1.2) using the finite difference method with two different boundary conditions : (i) a wall with uniform temperature, i.e. T_w= constant; and (ii) a uniformly heated wall, i.e. q=constant. Results are presented on graphs which show spatial distributions of dimensionless temperature $\theta(R,X)$, local Nusselt number Nu(X), and mean Nusselt number $Nu_m(X)$.

1.3.3 PROBLEMS WITH CIRCUMFERENTIAL VARIATION

All the above mentioned studies related to Graetz and Leveque methods are based on the simple boundary conditions where there is no circumferential variation at the wall-fluid interface. Moreover, the fluid temperature at the inlet (the step change in wall condition) is assumed to be uniform. For example, water at uniform temperature flows into a step change in wall temperature or wall heat flux.

There is axial symmetry in the tube because the boundary conditions do not vary in the circumferential direction.

Reynolds [14] obtained the solutions (temperature distributions) for any prescribed heat flux $q(\phi)$ around the circumference of a circular tube, without axial variation. He first obtained the solution corresponding to heat transfer across a small portion of the circumference as a Fourier series, and then obtained the solutions for arbitrary peripheral heat flux using superposition. This solution, however, does not describe the temperature profile development near the tube entrance, but only the peripheral distribution of the thermally developed flow further down the tube.

Bhattacharyya and Roy [15] took one further step in the arbitrary wall heat flux problem. First, they expressed the variable circumferential heat flux as a Fourier series in ϕ, the peripheral angle, and obtained the temperature distribution in the thermal entrance region. The solution is of the form

$$t(R,\phi,X) = k(T - T_{in})/(\bar{q}a)$$
$$= t_1(X) + t_2(R) + t_3(R,\phi) + t_4(R,\phi,X) \ , \qquad (1.6)$$

where $\bar{q}$ is the peripheral average wall heat flux, and

$$\bar{q}\ [\ 1 + \sum_{m=1}^{\infty} (a_m \cos m\phi + b_m \sin m\phi)] = k\ \partial T/\partial R = q \qquad (1.7)$$

represents the wall heat flux which is a function of the angle only. Applying Duhamel's superposition theorem, the

solution for an arbitrary wall heat flux distribution

$$q(\phi,X) = \bar{q}(X)[1 + \sum_{m=1}^{\infty} (a_m(X)\cos m\phi + b_m(X)\sin m\phi)] \qquad (1.8)$$

can be obtained. The solution is expressed in terms of an infinite series of eigenvalues and eigenfunctions. This work will be further discussed in Section 3.2.

1.3.4 CONJUGATED PROBLEM

Rather than using *a priori* fluid boundary conditions and obtaining the solution for the fluid only, the conjugated problem is formulated for the entire solid-fluid medium system, and a solution for both the fluid and solid temperature is obtained.

Luikov et al. [16] solved the conjugated problem for the circular tube. However, no numerical results were presented for the complicated closed-form solution.

Mori et al. [17] considered two thermal boundary conditions at the outside wall of the circular tube : (1) constant heat flux, (H2), and (2) constant temperature, (T). [1] They assumed the wall-fluid interface temperature distribution in the axial direction as a power series with unknown coefficients. The solution to the energy equation for the fluid was then obtained by superposing the Graetz solution. Equating the temperature and heat fluxes across the interface of the solid and fluid media they obtained the unknown coefficients for the power series. A conclusion

---

[1] See Table 2.1

relevant to the present work is that for a "thin" wall with constant heat flux specified at the outside wall, the local Nu(x) approaches that for the conventional (H2) convection problem. For a "thick" wall, however, it approaches the (T) solution because axial heat conduction tends to equalize the temperature inside the wall. A wall may be considered thin when $\gamma/L \leq 0.0001$ for $R_w \geq 2\times10^{-7}$ and when $\gamma/L \leq 0.001$ for $R_w \geq 10^{-5}$ [3].

Faghri and Sparrow [18] considered the effect of simultaneous wall and fluid axial conduction in a hydrodynamically developed laminar flow. Since only the thin-walled tube was considered, the radial temperature gradient in the wall was neglected. The problem was also considered to have no circumferential dependence because of symmetry around the axis. The circular tube considered had an insulated region ($x < 0$) and a region of direct heating ($x \geq 0$) where the heat flux at the outside wall of the tube was constant. Solutions were obtained by an elliptic-finite difference method employing an iterative scheme which dealt consecutively with the fluid and the tube wall. Plots of the axial distribution of the convective heat flux q, wall and bulk mean temperatures, T_w and T_m respectively, and Nusselt number were presented. Those graphs show that axial conduction depends on the Peclet number, Pe, and the dimensionless wall conductance parameter $B = k_w\gamma/ka$. Substantial amounts of convective heat transfer can occur along the non-directly heated portion ($x < 0$) of the tube

because of wall conduction. These effects of preheating are propagated downstream by the flowing fluid, so there is a substantial increase in both the wall and bulk temperatures all along the tube. It was found that the effect of wall conduction can readily overwhelm the effect of fluid axial conduction. In the region of direct heating ($x \geq 0$), the Nusselt number attains a fully developed value of 48/11, independent of axial conduction.

Barozzi and Pagliarimi [19] analysed the interaction between convection and axial heat conduction along the tube wall assuming a convective boundary condition at the outer face of the tube. They considered a wall whose thickness possessed periodic step variations in the axial direction. An iteratie procedure was set up starting with guessed distribution of local Nusselt no. and fluid bulk mean temperature, and temperature distribution in the solid region was determined by the finite element method. Their results show that axial wall heat conduction has a definite influence on heat flux $q(x)$ and the Nusselt no. $Nu(x)$ distribution especially near the thermal inlet section. Step variations in the wall thickness produce periodic oscillation in the distribution of $Nu(x)$ and $q(x)$, whose amplitude nevertheless reduces in a relatively short downstream distance, where their profiles approach that of a uniform thickness wall. However, overall heat flux can accurately be predicted by ordinary methods disregarding axial conduction.

The above review, although by no means complete, provides an overall idea of the available results relevant to the present work. No work has been found in the literature that directly investigates the stitch welding effect on the Nusselt number, and hence on solar collector performance. The next chapter describes the modelling of the problem, concentrating on the convective heat transfer aspects for the two extreme cases mentioned in Section 1.2.

2. MATHEMATICAL MODEL

To analyze the heat transfer from the solar collector absorber plate to the water flowing through its spot-welded tube, a mathematical model describing the physical and geometrical situation must be developed. The applicable differential equations and boundary conditions for both the solid and fluid media are discussed in this chapter. Enormous simplification is obtained by restricting attention to a certain class of flows and by making certain assumptions. Those assumptions can be justified for the typical flat plate solar collector used in building and domestic water heating. The simplified mathematical model of the heat transfer process is presented, and other important terms are defined.

2.1 GOVERNING EQUATIONS

As the investigation involves heat transfer in a moving fluid medium, the three conservation equations in fluid mechanics have to be satisfied. They are presented here in vector form :

1. Conservation of **Mass** :-

$$D\rho/D\tau = -\rho\ \bar{\nabla} \cdot \bar{V} \quad ; \qquad (2.1)$$

2. Conservation of **Momentum** :-

$$\rho\, D\ \bar{V}\ /D\tau = \rho\ \bar{g} + \bar{\nabla} \cdot S \quad ; \qquad (2.2)$$

3. Conservation of **Internal Energy** :-

$$\rho\ DI/D\tau = -\ \bar{\nabla} \cdot \bar{q} + \text{heat sources} + S(\ \bar{\nabla}\ \bar{V}\ ) \quad ; \qquad (2.3)$$

where standard notations in vector calculus are used . $D(\ )/D\tau$ is the substantial derivative, where τ denotes time. S is the stress tensor and the term $S(\ \bar{\nabla}\ \bar{V}\ )$ represents the complete contraction [2]. The resultant of all body forces acting on the medium is represented by $\bar{g}$.

It should be noted that these equations are applicable to any continuum, solid as well as liquid. For a stationary solid, the energy equation becomes

$$\rho \partial I/\partial \tau = - \bar{\nabla} \cdot \bar{q}_s + \text{heat sources} . \qquad (2.4)$$

Solving the general equations (2.1) to (2.4) as they stand is very difficult. One can only hope to obtain reasonably applicable solutions for special idealized cases. A number of assumptions have been made in modeling the solar collector of interest, which can be justified by examining the physical parameters involved.

2.2 IDEALIZATIONS

A table of dimensions and relevant physical properties for a typical flat-plate solar collector is given in Appendix A. The following assumptions are made based on the figures given in the table.

1. Since the fluid medium is water and temperature variations are small ($\Delta T \simeq 10\ ^{o}C$), it is considered to be **incompressible** as well as Newtonian. Furthermore, other properties are assumed to stay constant.
2. The water flow is **laminar** because $Re = \bar{u}D/\nu \simeq 1{,}400$.

---

[2] See Appendix C

3. Dissipation can be neglected because flow velocity is only a few cm/s and Mach number is low.
4. No heat source is present in the fluid as only solar energy is being absorbed by the plate.
5. Although there is no hydrodynamic starting length at the tube entrance, the velocity profile development is known to lead the thermal profile development significantly. This can be seen by realizing that, for water at moderate temperature, the Prandtl number,

$$Pr = \frac{\nu}{a} = \frac{\text{momentum diffusivity}}{\text{thermal diffusivity}} \simeq 4 .$$

Therefore, the velocity profile can be assumed to be already fully developed at the entrance [4]. This results in enormous simplification because the well known **parabolic velocity profile** as shown in Figure 1.5, can be substituted directly into the energy equation without having to solve equations (2.1), (2.2) and (2.3) simultaneously. This assumption results in a conservative estimate of the heat transfer coefficient.[3]

6. Axial conduction is negligible. Dimensional analysis [18] shows that this is the case when the Peclet number is large (Pe = Re.Pr > 100). Further discussion is given in Appendix B.

---

[3] The heat transfer coefficient is greater with a uniform velocity profile, which is found in slug flows and at the duct inlet during simultaneous development of velocity and temperature profiles [20].

7. Only **steady state** performance is considered. Thus all the partial derivatives with respect to time, $\partial(\ )/\partial\tau$, can be discarded from the governing equations.

2.3 SIMPLIFIED EQUATIONS

Assuming the velocity profile of the fluid to be fully developed at the tube entrance, the radial velocity distribution is assumed to be known and invariant with axial distance. Due to circular symmetry, the velocity is also independent of peripheral angle. That is,

$$\vec{V} = u(R)\hat{i} = U[\ 1 - (R/a)^2]\ \hat{i}\ , \qquad (2.5)$$

where u is the axial component of the velocity, and U, which can be calculated from the mass flow rate[4] is the peak velocity of the flow. This parabolic profile is known as the **Poiseuille flow** velocity distribution for incompressible Newtonian fluid with constant properties. Its form is derived in detail in Burmeister [20].

As a consequence of the velocity distribution being known, the continuity and momentum equations need not be considered. Only the energy equations for both the fluid and solid media are of concern. For the solid media, under steady state conditions and with constant thermal conductivity

$$k_s\nabla^2 T = \text{sources}\ . \qquad (2.6)$$

For the absorber plate, the heat source is equal to the

---

[4] See Appendix A.

difference between the incoming solar radiation and the heat loss to the ambient through the resistance $1/U_L$.

For a Newtonian incompressible fluid, equation (2.3) reduces to

$$\rho \, DH/D\tau = Dp/D\tau + \text{heat sources} - \vec{\nabla} \cdot \vec{q} + \mu\Phi \ ,$$

where $H = I + p/\rho$ is the enthalpy per unit mass, and Φ is the dissipation function[5]. Applying the assumptions that the water properties stay constant, that no heat source is present, and that dissipation is negligible, the energy equation further reduces to [20] :

$$\rho \, c_p DT/D\tau = k\nabla^2 T \ . \qquad (2.7)$$

Substituting equation (2.5) directly into (2.7), the steady state energy equation for the fluid is found to be

$$U[1 - (R/a)^2] \, \partial T/\partial X = a\nabla^2 T \qquad (2.8)$$

where $a = k/\rho c_p$ is the thermal diffusivity.

Equation (2.8) is to be solved under certain boundary conditions as discussed in the next section.

2.4 THERMAL BOUNDARY CONDITIONS

A set of specifications describing temperature and/or heat flux conditions at the inside wall of the duct must be obtained to solve the fluid energy equation (equ.2.8). A large variety of these **thermal boundary conditions** can be

---

[5]See Appendix C for details.

specified for the classical problem concerning the thermal profile development. Shah and London [3] attempted to systemize the boundary conditions studied in the literature. A few well-studied cases are shown in Table 2.1.

In general, however, because of conduction in the tube wall, well-defined temperature or heat flux conditions are seldom encountered at the inside wall of the duct. Only in extreme cases can those conditions be specified. Two extreme cases exist for the water flowing through the spot-welded tube under study, determined by the "thickness" of the tube wall :

1. For a thick and highly conductive wall, the axial and peripheral conduction of heat from the welding spot to the rest of the wall is considerable compared to the radial heat transfer into the flowing water (Figure 2.1(i)). Conduction occurs until the whole tube wall comes to a uniform temperature.
2. For a thin and low conductive wall as shown in Figure 2.1(ii), the wall peripheral and axial conductance is negligible compared with the raidal conductance. Therefore, solar radiation being absorbed by the collector plate passes into the water only radially through the welding spots. Thus the flowing water is subject to a wall boundary which consists of spots of heat flux.

The definition of a "thin" wall has been given in Section 1.3.4.

For the idealized case (2), the boundary conditions can be depicted by mathematical expressions quite straight forwardly. Peripherally, the heating spots occupy the angular range $-\phi_c \le \phi \le \phi_o$. Where $\phi_o < \phi < (2\pi-\phi_o)$, the heat flux is zero. This distribution can be expressed in terms of a Fourier series,

$$f(\phi) = \begin{cases} Q_{sol}, & -\phi_o \le \phi \le \phi_o \\ 0, & \text{otherwise} \end{cases}$$

$$= (Q_{sol}\phi_o/\pi)\ [1 + \sum_{m=1}^{\infty} (a_m \cos m\phi)\ ]\ , \qquad (2.9)$$

where $a_m = 2(\sin m\phi_o)/(m\phi_o)$.

$f(\phi)$ is as shown in Figure 2.2. It should be noted that

$$Q_{sol}(\phi_o/\pi) = \bar{q}$$

is the peripheral mean heat flux through the wall.

Axially, the spots are of fixed length and are located at fixed intervals. The heat flux, as a function of both x and ϕ, can be expressed as follows :

$$q(\phi,x) = f(\phi)H(x) - f(\phi)H(x-x_1) + f(\phi)H[x-(x_1+x_s)]$$
$$- f(\phi)H[x-(2x_1+x_s)] + \ldots\ , \qquad (2.10)$$

where $H(x) = \begin{cases} 0, & x < 0 \\ 1, & x \ge 0 \end{cases}$

is the Heaviside unit step function. The illustration of $q(x,\phi)$ where $-\phi_o \le \phi \le \phi_o$ is in Figure 2.3.

Closed form solutions of reasonable applicability can be obtained only for the above two extreme cases, where the boundary conditions are clearly predefined. Extreme case (1) corresponds to the Graetz problem and its solution is well known. The analytical method and solutions for case (2) are the subject of the next chapter. The analytical results were checked against and supplemented with a numerical procedure which will be described in Chapter 4.

3. ANALYTICAL SOLUTIONS

The governing energy equation and associated boundary conditions for the heat transfer problem under study have been presented in Chapter 2. This chapter describes briefly the analytical methods of solutions available in the literature. The method employed in arriving at the solution for the extreme case (2) of Section 2.4 is detailed in this chapter. The principle of **superposition** is shown to be of great usefulness in this kind of linear problem.

3.1 OVERVIEW OF ANALYTICAL SOLUTIONS

The analytical solutions for hydrodynamically developed thermal entrance flows are obtained primarily by the following four kinds of methods :

1. Separation of Variables and Similarity Transformation methods;
2. Variational Methods;
3. Conformal Mapping Method; and
4. Simplified Energy Equation Method.

These methods and their sources in the literature have been briefly described by Shah and London [3]. Attention will be given here to the separation of variables method, which was employed in solving the present problem.

3.2 SEPARATION OF VARIABLES METHOD

The separation of variables method was used in the first study by Graetz [5] of the thermal entrance region of a circular tube. Many of the solutions of later work were obtained by similar methods. The method involves separating the variables in the energy equation (2.8) and determining the eigenvalues and constants of the resulting ordinary differential equations by various approaches. The solution is presented in terms of an infinite series involving eigenvalues, eigenfunctions, and constants. Examples of work where this method is employed to the circular duct are that by Reynolds [14], Sellars et al.[8], and by Bhattacharyya and Roy [15], which have been cited in Section 1.3.

The work by Bhattacharyya and Roy can be described in two parts. First, the temperature solution was obtained for the thermal entrance region for developed laminar flow in a circular tube with variable circumferential wall heat flux. The energy equation is rewritten here, in cylindrical co-ordinates:

$$U(1-R^2/a^2)\,\frac{\partial T}{\partial X} = \alpha\left(\frac{\partial^2 T}{\partial R^2} + \frac{1}{R}\frac{\partial T}{\partial R} + \frac{1}{R^2}\frac{\partial^2 T}{\partial \phi^2}\right), \qquad (3.1)$$

where the axial conduction term $\partial^2 T/\partial X^2$ has been omitted. The boundary conditions are:

$$\text{at } R = a : k\partial T/\partial R = q = \bar{q}\left[1 + \sum_{m=1}^{\infty} g_m(\phi)\right], \qquad (3.2a)$$

where $g_m(\phi) = a_m \cos m\phi + b_m \sin m\phi$, (3.2b)

and $\bar{q}$ is the mean wall heat flux over the circumference;

at $X = 0 : T = T_{in}$. (3.2c)

The dimensionless forms of the above equations were expressed as

$$(1-r^2)\frac{\partial t}{\partial x} = \frac{\partial^2 t}{\partial r^2} + \frac{1}{r}\frac{\partial t}{\partial r} + \frac{1}{r^2}\frac{\partial^2 t}{\partial \phi^2} \quad , \tag{3.3}$$

$$r = 1 : \partial t/\partial r = 1 + \sum_{m=1}^{\infty} g_m(\phi) \quad , \tag{3.4}$$

$$x = 0 : t = 0 \quad , \tag{3.5}$$

where $t = k(T - T_{in})/\bar{q}a$,

$x = \alpha X/Ua^2 = X/a.Pe$,

$r = R/a$. (3.6)

The equations (3.3) to (3.5) were solved by separation of variables and the result was :

$$t = 4x + r^2 - r^4/4 - 7/24 + \sum_{m=1}^{\infty} (r^m/m) g_m(\phi) - \sum_{s=1}^{\infty} c_{0s} R_{0s} \exp(-\beta_{0s}^2 x) - \sum_{m=1}^{\infty}\sum_{s=0}^{\infty} c_{ms} R_{ms} g_m(\phi) \exp(-\beta_{ms}^2 x) \quad , \tag{3.7}$$

where $R_{ms}(r, \beta_{ms})$ are eigenfunctions, β_{ms} are eigenvalues, and c_{ms} are the corresponding constants. For details of the mathematics the reader is referred to Ref.[15] where useful values of the eigenfunctions and eigenvalues are given.

The advantage of dimensionalizing the variables as in equations (3.6) is perhaps best seen from the expression of the Nusselt number, i.e. the dimensionless heat transfer

coefficient. By definition, the **local Nusselt number** is given by :

$$Nu(\phi,X) = \{ q(\phi,X)/[T_w(\phi,X) - T_m(X)] \}(D/k) . \qquad (3.8)$$

The term in braces is the local heat transfer coefficient, commonly denoted by h. Expressing in terms of the dimensionless temperatures, with

$$\dot{m}c_p\Delta T_m = \bar{q}(2\pi a)\Delta X \Longrightarrow t_m = 4x ,$$

equation (3.8) takes the form

$$Nu(\phi,x) = \frac{2[1 + \sum_{m=1}^{\infty} g_m(\phi)]}{11/24 + \sum_{m=1}^{\infty} [g_m(\phi)/m] - \sum_{s=1}^{\infty} c_{0s}R_{0s}(1,\beta_{0s}) \exp(-\beta_{0s}^2 x) - \sum_{m=1}^{\infty} \sum_{s=0}^{\infty} [c_{ms}R_{ms}(1,\beta_{ms})g_m(\phi) \exp(-\beta_{ms}^2 x)]} . \qquad (3.9)$$

The **peripheral average Nusselt number**, according to the definition of Shah and London [3], is given by:

$$Nu_p(X) = \{ \bar{q}(X)/[T_{wm}(X) - T_m(X)] \}(D/k) , \qquad (3.10)$$

where $\bar{q}(X) = (1/2\pi)\int_0^{2\pi} q(\phi,X)d\phi$,

$T_{wm}(X) = (1/2\pi)\int_0^{2\pi} T_w(\phi,X)d\phi$.

According to the expression of t in equation (3.7), the peripheral average Nusselt number can also be written as

$$Nu_p(x) = \frac{2}{11/24 - \sum_{s=1}^{\infty} c_{0s}R_{0s}(1,\beta_{0s}) \exp(-\beta_{0s}^2 x)} . \qquad (3.11)$$

Whereas the first part of Bhattacharyya and Roy's work deals with a tube with no axial variation in wall heat flux

besides the entrance step change, the second part involves obtaining the solution for an arbitrarily heated tube wall. The solution was obtained by applying Duhamel's superposition formula on equation (3.7). The resulting series solution involves complicated integrals and is impractical for engineering calculation. A simpler superposing technique is applicable to the present problem.

3.3 SOLUTION FOR "THIN" TUBE USING SUPERPOSITION

Consider a boundary value problem whose governing differential equation is

$$A(t) = 0 ,$$

where A is a **linear operator**, and has derivative boundary conditions

$$t'\big|_{bdry} = H_1 + H_2 + \dots + H_{2N} . \qquad (*)$$

Suppose there exist 2N functions $t_1, t_2 \dots t_{2N}$, satisfying the following:

$$A(t_i) = 0 ,$$

$$t_i'\big|_{bdry} = H_i , \quad i = 1,2,\dots,2N ,$$

then their sum, $\sum_{i=1}^{2N} t_i$, will be the solution to (*) because it satisfies the differential equation as well as the boundary conditions :

$$A\left(\sum_{i=1}^{2N} t_i\right) = \sum_{i=1}^{2N} [A(t_i)] = 0 ,$$

$$\left(\sum_{i=1}^{2N} t_i\right)'\Big|_{bdry} = \sum_{i=1}^{2N} \left(t_i'\Big|_{bdry}\right) = H_1 + H_2 + \ldots + H_{2N} .$$

Substituting the following operator for A in (*) :

$$\left[\frac{\partial^2}{\partial r^2} + \frac{1}{r}\frac{\partial}{\partial r} + \frac{1}{r^2}\frac{\partial^2}{\partial \phi^2} - (1-r^2)\frac{\partial}{\partial x}\right] ,$$

and letting $H_1 = f(\phi)H(x)$,

$$H_2 = - f(\phi)H(x-x_1) ,$$

$$H_3 = f(\phi)H[x-(x_1+x_s)] , \text{ etc,}$$

the problem posed by equations (3.3) and (2.10) is the same as the system (*). The solution is then

$$t(r,\phi,x) = \sum_{i=1}^{2N} t_i(r,\phi,x) , \qquad (3.12)$$

where t_1 is identical to the function t in equation (3.7),

$$t_2 = - t_1(r,\phi,x-x_1)H(x-x_1) ,$$

$$t_3 = t_1(r,\phi,x-(x_1+x_s))\, H[x-(x_1+x_s)] , \text{ etc.} \qquad (3.13)$$

$t_1(r,\phi,x)$ of equation (3.12), with appropriate constants, describes the temperature distribution of a steady laminar flow entering a circular tube which is heated over a fraction of its circumference, a situation illustrated by Figure 3.1. Axially, the heating starts at x=0 and is invariant with distance. The mathematical expression for this boundary condition is

$$q(\phi,x) = f(\phi)\, H(x) ,$$

where $f(\phi)$ is given in equation (2.9).

The Nusselt number corresponding to solution (3.12) can also be found by superposition:

For $-\phi_o \leq \phi \leq \phi_o$,

$$1/Nu(\phi,x) = \sum_{i=1}^{2N} (t_{w,i} - t_{m,i})/2 = \sum_{i=1}^{2N} [1/Nu_i(\phi,x)] \ , \qquad (3.14)$$

where $Nu_1(\phi,x)$ is given by equation (3.9), and

$$1/Nu_2(\phi,x) = (t_{w,2} - t_{m,2})/2 = -H(x-x_1) \ / \ Nu_1(\phi,x-x_1) \ ,$$

$$1/Nu_3(\phi,x) = (t_{w,3} - t_{m,3})/2 = H[x-(x_1+x_s)]/Nu_1(\phi,x-(x_1+x_s)),$$

etc. (3.15)

For other values of ϕ, the Nusselt number is zero since there is no heat flux through the wall.

The peripheral average Nusselt number $Nu_p(x)$ can be found by similar superposition on equation (3.11). The effect on the Nusselt numbers of neglecting fluid axial conduction is discussed in Appendix B.

3.4 GRAPHICAL ILLUSTRATION OF ANALYTICAL RESULTS

The boundary condition (2) of Section 2.4 depicts the extreme situation where the tube wall is so thin that solar energy passes into the water only radially through the welding spots. The analytical solution for the temperature distribution in this case is given by equations (3.12) and (3.13). With 1/8 of the tube circumference being welded continuously along its length[6], $a_m = \sin(m\phi_o)(2/m\phi_o)$ and $b_m = 0$

---

[6] The spot angle of 45°, i.e. $\phi_o = \pi/8$ was chosen arbitrarily to enable comparison with other cases.

in the function $g_m(\phi)$ which appears in the expression of t_1. The solution is written here for r=1:

$$t(1,\phi,x) = 4x + 11/24 + \sum_{m=1}^{\infty} [a_m \cos m\phi)/m] - \sum_{s=1}^{\infty} c_{0s} R_{0s}(1,\beta_{0s}) \exp(-\beta_{0s}^2 x) - \sum_{m=1}^{\infty} \sum_{s=0}^{\infty} [c_{ms} R_{ms}(1,\beta_{ms}) (a_m \cos m\phi) \exp(-\beta_{ms}^2 x)]. \quad (3.16)$$

The value of t at r = 1 was plotted against x for various values of ϕ in Figure 3.3. This diagram shows the axial development of the wall temperature at various angular positions. As expected, the temperatures at those angular positions which are directly heated increase sharply near the entrance. Further downstream, the temperatures at all angles assume a linear relationship with distance, a situation termed as **thermally developed.** There is a significant difference in temperature between the angular position which is just inside the directly heated region ($\phi=\pi/10$) and the one which is just outside ($\phi=2\pi/10$).

The local and peripheral average Nusselt numbers for the above situation were plotted against x in Figure 3.4. The local Nusselt number $Nu(\phi,x)$ was only shown for two angular positions inside the welded region, since its value is zero for those positions outside that region. It might be noticed that $Nu_p(x)$ is identical to that of a uniformly heated tube. This should come as no surprise if the definition of $Nu_p(x)$ (equation(3.10)) is understood. In any case, the thermal entrance has an effect of increasing

sharply the heat transfer coefficient, as can be seen from the Nusselt numbers near x=0.

To illustrate the effect of superposition on equation (3.16), a tube as in Figure 3.2 with two welding spots occupying 60% of its length was considered. The spot angle was kept at 45°, i.e. $\phi_o = \pi/8$. The solution becomes, for the wall temperature,

$$t(1,\phi,x) = \sum_{i=1}^{2N} t_i(1,\phi,x) \ ,$$

where t_1 is given by equation (3.16),

$$t_2 = -t_1(1,\phi,x-x_1)\ H(x-x_1) \ ,$$

$$t_3 = t_1(1,\phi,x-(x_1+x_s))\ H(x-(x_1+x_s)) \ ,$$

$$t_4 = -t_1(1,\phi,x-(2x_1+x_s))\ H(x-(2x_1+x_s)) \ ,$$

etc,

with $2x_1 = 0.6$(tube-length) ,

$2x_s = 0.4$(tube-length) .

$t(1,\phi,x)$ was plotted against x in Figure 3.5. It can be noted that the axial temperature fluctuation is much more pronounced in the range of ϕ that is directly heated. Again, there is a significant difference in temperature from $\phi=\pi/10$ to $\phi=2\pi/10$. The general trend of temperature increasing downstream can also be observed.

It was intended to compare the mean Nusselt number Nu_m between different welding spot configurations, given a fixed total weld length and a fixed spot angle, and hence a fixed total heat input. The tube could be welded to the absorber plate at any number of equally spaced and identical

stitches, while a stitch angle of 45° and a total weld length of 60% of the tube length were arbitrarily chosen as invariants. Results of two different cases were shown in Figures 3.6 (i) and (ii), where the tube was welded at : (i) a single stitch; and (ii) 4 stitches, respectively. It can be observed that a higher number of stitches results in a higher mean Nusselt number since they introduce more "thermal entrance effect" to the temperature profile.

The correctness of the analytical results can be checked by solution obtained through numerical methods. The next chapter describes the finite difference formulation of the same problem. The finite difference results were compared with those described in this chapter.

4. NUMERICAL SOLUTIONS

The analytical solutions and results presented in the last chapter are those for the idealized boundary condition where the fluid is bounded by spots of heat flux at the wall. This chapter describes a numerical approach to the same boundary value problem. The results serve both as a check and a supplement to the analytical solutions. The basic assumptions outlined in Section 2.2, and hence the simplifications, are retained, and the same dimensionless variables defined in equation (3.6) are used.

4.1 OVERVIEW OF NUMERICAL METHODS

The thermal entrance solutions for hydrodynamically developed flows can be obtained by several methods. The analytical methods have been outlined in Section 3.1, while the numerical methods can be classified as follows:

1. Finite Difference Methods;
2. Monte Carlo Method; and
3. Finite Element Method.

A brief description of these methods and their sources in the literature can be found in Shah and London [3]. The method used in the present work solves the finite difference formulation of the dimensionless energy equation using an iterative technique. The next section is devoted to the details of this formulation.

4.2 FINITE DIFFERENCE FORMULATION

A program was developed to solve the 3-dimensional equation (3.3) numerically, and hence the temperature distribution of the fluid inside the tube was obtained. The Nusselt number distribution was then computed directly from the temperature values using the definitions in equations (3.8) to (3.10).

The tube volume was divided by radial, circumferential, and axial grids, with corresponding grid spacing of Δr, $\Delta\phi$, and Δx, respectively, as shown in Figure 4.1. The location of each node was defined by a cylindrical coordinate in terms of the grid numbers. Thus the temperature at all nodes can be stored in a 3-dimensional array, $t(N_r, N_\phi, N_x)$, where

$N_r = 0, 1, \ldots M_r$ is the radial grid number,

$N_\phi = 0, 1, \ldots M_\phi$ is the circumferential grid number,

and $N_x = 0, 1, \ldots M_x$ is the axial grid number of the node.

Written in finite difference form, the energy equation takes the following form:

$$\frac{t_3 - 2t_5 + t_1}{(\Delta r)^2} + \frac{1}{r}\frac{t_3 - t_1}{2\Delta r} + \frac{1}{r^2}\frac{t_2 - 2t_5 + t_4}{(\Delta\phi)^2} = (1-r^2)\frac{t_0 - t_5}{\Delta x}, \tag{4.1}$$

where $t_0, \ldots, t_5$ represent the temperatures at the locations indicated in Figure 4.2. This equation is written for the point (N_r, N_ϕ, N_x) whose temperature is t_0, and $r = N_r \cdot \Delta r$ is the dimensionless radial coordinate of that point. Two different cases need to be considered separately:

(i) $r \neq 0$:

$$t_o = [a_1 t_1 + a_2(t_2+t_4) + a_3 t_3 + a_5 t_5] / a_o \ , \quad (4.2)$$

where $a_o = (\Delta r)^2(1-r^2) / \Delta x$,

$a_1 = 1 - \Delta r/2r$,

$a_2 = (\Delta r/r\Delta\phi)^2$,

$a_3 = 1 + \Delta r/2r$,

$a_5 = - 2 - 2a_2 + a_o$.

(ii) $r = 0$:

$$\nabla^2 t = 4(t_{avg} - t_5)/(\Delta r)^2 \ , \quad (4.3)$$

where $t_{avg} = \sum_{N_\phi=0}^{M_\phi} t(1,N_\phi,N_x-1)/(M_\phi+1)$

is the average temperature at the immediate neighborhood of the tube center-line. So

$$t_o = (4\Delta x/\Delta r^2)t_{avg} + (1 - 4\Delta x/\Delta r^2)t_5 \ . \quad (4.4)$$

An imaginary surface $N_r = M_r + 1$ was added outside the tube wall to implement the temperature gradient at the wall as determined by the pre-described heat flux. The temperature at a node on that surface was determined by whether the node's peripheral and axial location was within that of a welding spot:

(i) within spot : $\Delta t/\Delta r = \pi/\phi_o$,[7]

$$t(M_r+1,N_\phi,N_x) = t(M_r-1,N_\phi,N_x) + 2\Delta r(\pi/\phi_o) \ ; \quad (4.5)$$

---

[7] $(1 + \sum_{m=1}^{\infty} a_m \cos m\phi) = \pi/\phi_o$ when $-\phi_o \leq \phi \leq \phi_o$.

(ii)not within spot : $\Delta t/\Delta r = 0$,

$$t(M_r+1,\ N_\phi,\ N_x) = t(M_r-1,\ N_\phi,\ N_x)\ . \qquad (4.6)$$

Therefore, the temperature at each node can be expressed in terms of the temperatures at its neighborhood nodes. After initializing the 3-dimensional array of temperatures with a non-zero function, a new value for each node was obtained using equations (4.2) to (4.6). Evaluation of temperatures was done one circular cross-section after another, starting from the tube entrance $N_x=0$. The temperature at the entrance was always kept at 0 to conform with the boundary condition $t(r,\phi,0) = 0$. After the temperature at all nodes had been updated, the process was repeated until deviation between two successive evaluations was less than 0.5% at any node. Convergence was then considered attained and the array $t(N_r,N_\phi,N_x)$ would contain the solution temperature distribution.

4.3 CALCULATION OF NUSSELT NUMBERS

Having obtained the temperature distribution throughout the fluid body, the heat transfer coefficient h, and its dimensionless form, the Nusselt number, were computed according to definitions. The definition of the peripheral average and mean Nusselt numbers are reproduced here:

$$Nu_p(x) = \begin{cases} 2/[t_{wm}(x)-t_m(x)], & \text{if x falls within a spot;} \\ 0\ , & \text{otherwise,} \end{cases} \qquad (4.7)$$

$$Nu_m(x) = (1/x)\int_0^x Nu_p(x)dx \ , \qquad (4.8)$$

where $t_w(\phi,x)$= dimensionless local wall temperature,

$t_{wm}(x)$ = peripheral average wall temperature,

$= (1/2\pi)\ \int_0^{2\pi} t_w(\phi,x)d\phi$,

$t_m(x)$ = bulk mean temperature,

$=(1/UA)\ \int_A (ut)dA = (2/\pi a^2)\ \int_A (1-r^2)\ t\ dA$,

and x-outside-spot if $x \geq nx_1+(n-1)x_s$ and $x < n(x_1+x_s)$

where n = 1,2,..... ,

x-within-spot otherwise. (4.9)

In finite difference formulation, the above integrals were computed as follow:

$$t_{wm}(N_x) = \frac{t(M_r,0,N_x) + 2\sum_{N_\phi=1}^{M_\phi-1} t(M_r,N_\phi,N_x) + t(M_r,M_\phi,N_x)}{2\ M_\phi} \ , \qquad (4.10)$$

$$t_m(N_x) = (2/\pi)\{\sum_{N_r=1}^{M_r} [UTDA(N_r,0,N_x) + 2\sum_{N_\phi=1}^{M_\phi-1} UTDA(N_r,N_\phi,N_x) + UTDA(N_r,M_\phi,N_x)] + t(0,N_\phi,N_x)\ \pi(\Delta r)^2\} \ , \qquad (4.11)$$

where $UTDA(N_r,N_\phi,N_x) = (1-r^2)\cdot t(N_r,N_\phi,N_x)\cdot(\Delta\phi/2)(r_2^2-r_1^2)$,

and $r_1 = N_r\cdot\Delta r$, $r_2 = (N_r+1)\cdot\Delta r$. (4.12)

4.4 PRELIMINARY RESULTS OF NUMERICAL PROCEDURE

With the basic algorithm as outlined in the previous two sections, the computational program was developed in several stages. The results of each stage were checked against those obtained by other methods, if available,

before another stage was developed. This section presents those results stage by stage.

First, the simplest case of a uniformly heated tube wall was taken as the boundary condition to test the program. This problem has been well studied and results have been tabulated in Shah and London[3]. The computed temperature, as expected, does not depend on the peripheral angle ϕ, and its value at various radial coordinates r was plotted against x in Figure 4.3. Compared with the tabulated values of the wall temperature, the finite difference result was found to be higher near the entrance, although the two results converge at large x (x>80). This discrepancy at the entrance was found in all the later results and it was found to be due to the coarseness of the grid system. The Nusselt number ($Nu(\phi,x) = Nu_p(x)$ in this case) is shown in Figure 4.4, with Shah and London's values plotted against the same axes.

Next, a wall was chosen to have 1/8 of its circumference directly heated (the welding spot) and insulated everywhere else. This situation is as shown in Figure 3.1. Figure 4.6 shows the wall temperature plotted against x, for various angular positions at the wall as shown in Figure 4.5. Compared with the analytical results for the same problem[8], the entrance discrepancy can be observed as in the case of the uniformly heated tube. In this case as well as in that of the uniformly heated tube, a

---

[8]Shown in Figure 3.3.

linear relationship between t and x can be observed far downstream, a region where the flow is described as thermally developed. The reader is cautioned that when comparing the dimensionless temperatures between different cases, for example between those in Figures 4.3 and 4.6, it should be remembered that the definition of t depends on the value of $\bar{q}$ which in turn depends[9] on ϕ_o.

Further complicating the boundary conditions by introducing axial step changes of heat flux, the problem shown in Figure 3.2 was solved by the program. The wall temperature obtained is shown in Figure 4.7. The temperature profiles agree well with the analytical results[10] except at a short distance downstream from all the step changes. The temperature distributions further inside the tube at various radial coordinates are also shown : Figure 4.8 for r=4/5 and Figure 4.9 for r=1/5. The inner fluid close to the wall (r=4/5) has a substantially lower temperature than that at the wall, especially at those angular positions within a welding spot (ϕ=0 and $\phi=\pi/10$). This radial temperature gradient is what permits the heat flux from the weld to pass into the inner fluid. Close to the tube centre-line, at r=1/5, the temperature hardly rises or fluctuates with flow length. Furthermore, circumferential heat transfer is much less pronounced in the inner fluid as can be seen from the smaller circumferential temperature gradient. It should be commented that there is no thermally developed region in

---

[9] $\bar{q}=Q_{sol}(\phi_o/\pi)$

[10] Shown in Figure 3.5.

this case because there is axial variation of boundary conditions all along the flow length.

Finally, the flow length to be considered was halvened to allow finer divisions of the grids without much increase of memory space, and the same two cases which resulted in Figures 3.6(i) to (ii) were solved by the program. Whereas the Nusselt numbers were calculated using simple analytical expressions outlined in Section 3.3, they were now computed directly from definitions, using equations (4.7) to (4.11). As can be seen from Figures 4.10(i) and (ii), the numerical method produced the same results as the analytical method.

That the numerical solutions converge to the analytical ones as grid spacing gets finer reassures that both methods work. Further results appropriate to collector efficiency evaluation are shown in the next chapter. Implication of those results to collector performance will also be elaborated.

5. APPLICATION TO COLLECTOR EFFICIENCY FACTOR

As mentioned in Chapter 1, the collector efficiency factor F' is given by

$$F' = \frac{1/U_L}{W\{\ 1/[U_L(b+(W-b)F)] + 1/C_b + \gamma/(\pi Dk_w) + 1/(\pi Dh)\}} . \tag{1.1}$$

The heat transfer coefficient h appropriate to this expression was determined from a definition for Nu(x) slightly different than that in equation (3.10). The relationship between this Nu and x was calculated for various spot angles ($2\phi_o$), welded percentage w of tube length, and total number N of spots along a tube. Choosing a spot angle as invariant, the relationship between F' and spot configurations (i.e. w and N) can be illustrated.

The results for the "thick" tube all tend to the uniform wall temperature case since the heat transfer coefficient does not depend on spot configuration. This result can be regarded as the upper limit of actual performance. On the other hand the results for the "thin" tube are more interesting because spot configuration is important in determining F'. This result serves as the lower limit of actual performance, and will be the major concern of this chapter.

5.1 HEAT TRANSFER COEFFICIENT BASED ON BOND TEMPERATURE

The common definition of $Nu_p(x)$ (e.g. equation(3.10)) is based on the difference between the peripheral average wall temperature and the bulk mean temperature of the fluid. A careful analysis of the classical fin problem reveals that a Nusselt number based on the difference between the bond temperature and the bulk mean temperature should be used in conjunction with equation (1.1). The result of the classical fin problem associated with the flat plate collector with "thin" tubes is briefly outlined below.

The useful energy gain per unit of length in the flow direction for a collector tube can be shown [1] to be

$$q_u = [(W-b)F + b][Q_{sol} - U_L(T_b-T_a)] , \qquad (5.1)$$

where Q_{sol} is the solar energy absorbed by unit area of the plate, T_b is the temperature at the plate-tube bond, T_a is the ambient temperature, and the remaining terms are defined in Section 1.1. Ultimately, the useful gain q_u must be transferred to the fluid. The resistance to heat flow to the fluid comprises that of the bond, the tube wall, and the fluid to tube resistance. The useful gain can be expressed in terms of these three resistances as

$$q_u = \frac{T_b - T_m}{1/C_b + \gamma/\pi D k_w + 1/\pi D h} .$$

It has been shown [2] that the bond resistance $1/C_b$ is negligible compared with the other resistances. Furthermore, since the tube wall is assumed extremely thin, the radial

resistance offered by the wall $\gamma/\pi Dk_w$ is also negligible. The useful energy gain per unit of flow length per tube is

$$q_u = \frac{T_b - T_m}{1/\pi Dh} . \qquad (5.2)$$

But $q_u(X) = 2\pi a\bar{q}(X)$, so the following familiar form is obtained :

$$h_b(X) = \bar{q}(X) \; / \; [T_b(X) - T_m(X)] . \qquad (5.3)$$

At the axial positions where no welding is done, a thin layer of air between the tube and the fin offers a large radial resistance to heat flow, and both $\bar{q}$ and h_b in the equation can be taken as zero. Thus, equation (5.3) applies whether X falls within a welding spot or not. Furthermore, since the bond and the wall resistance are both negligible, the fluid temperature at R = a and ϕ = 0 can be taken as the bond temperature (Figure 5.1). Therefore the mean heat transfer coefficient over the entire flow length L is

$$h_{bm} = \frac{1}{L} \int_0^L \frac{\bar{q}(X)dX}{T(a,0,X) - T_m(X)} . \qquad (5.4)$$

In dimensionless form, equation (5.4) becomes

$$h_{bm} = (k/D)Nu_{bm}$$

$$= (k/Dl) \int_0^1 Nu_b(x)dx , \qquad (5.5)$$

where $Nu_b(x) = 2/[t(1,0,x)-4x]$, if x-within-spot,

$= 0$, if x-outside-spot, (5.6)

and $l = L/a \cdot Pe$.

Solving equation (5.2) for T_b and substituting into equation (5.1), one obtains

$$q_u = WF'[Q_{sol} - U_L (T_m - T_a)] ,$$

where $$F' = \frac{1/U_L}{W\{1/[U_L(b+(W-b)F)] + 1/(\pi D h_{bm})\}} .$$ (5.7)

The same expression for F' can be obtained from equation (1.1) if the resistances due to the bond and the tube wall are neglected.

The Nusselt no. based on bond temperature Nu_b as in equation (5.6) was calculated using the series solution and superposition method discussed in Chapter 3. The collector efficiency factor can then easily be calculated. Before comparing the value of F' for different welding-spot configurations, one configuration was arbitrarily chosen to illustrate the bahaviour of $Nu_b(x)$ and $Nu_{bm}(x)$ using this definition. This is illustrated in the next section.

5.2 BEHAVIOUR OF NU(X) FOR A CONTINUOUSLY WELDED TUBE

To calculate $Nu_b(x)$, the dimensionless temperature difference $t(1,0,x)-4x$ is required. For a continuously welded tube with spot angle $2\phi_o$, this difference can be found using equation (3.16) :

$$Nu_b(x) = 2/[t(1,0,x)-4x]$$

$$= \frac{2}{[\ 11/24 + \sum_{m=1}^{\infty} a_m/m - \sum_{s=1}^{\infty} c_{0s}R_{0s}\exp(-\beta_{0s}^2 x) \sum_{m=1}^{\infty}\sum_{s=0}^{\infty} c_{ms}R_{ms}a_m\exp(-\beta_{ms}^2 x)\ ]} \quad (5.8)$$

Nu_b plotted against 1000x appears in Figure 5.2 for various values of ϕ_o. The case $\phi_o = \pi$ corresponds to the well known case of a uniformly heated wall, where $t(1,0,x)$ equals the peripheral average wall temperature. Thus the Nusselt curve for $\phi_o=\pi$ coincides with the accepted $Nu_p(x)$ curve for a uniformly heated tube [11] and approaches the expected asymptotic value of 48/11.

As the spot angle $2\phi_o$ decreases, so does the Nusselt number based on bond temperature. This is not the case for the Nusselt number based on peripheral average wall temperature $Nu_p(x)$, which does not depend on ϕ_o but conforms with the uniformly heated case. It is obvious that the larger the spot angle, the higher the mean heat transfer coefficient based on bond temperature h_{bm} and hence the efficiency factor F'. This increase in F' is obtained at the cost of more welding.

5.3 BEHAVIOUR OF NU(X) OF SPOT WELDED TUBE

A larger spot angle results in a higher F' for the spot-welded as well as the continuously welded tube. For the spot-welded tube, the higher the percentage w of tube length

---

[11] Shown in Figure 3.4

being welded to the absorber plate (from which heat flows in through the spots), the higher is h_{bm}. Furthermore, for a given w and ϕ_o, distributing the welding into a larger number N of spots results in a higher h_{bm}. This is because more spots introduce more thermal entrance effect.

The expression (5.8) for the continuously welded tube can be superposed to obtain the $Nu_{bm}(x)$ and hence h_{bm} for the spot-welded tube. Following a similar argument outlined in Section 3.3, one obtains

$$1/Nu_b(x) = \sum_{i=1}^{2N} [1/Nu_{ib}(x)] , \qquad (5.9)$$

where $Nu_{1b}(x)$ is given by equation (5.8), and

$$1/Nu_{2b}(x) = -H(x-x_1) / Nu_{1b}(x-x_1) ,$$

$$1/Nu_{3b}(x) = H[x-(x_1+x_s)] / Nu_{1b}(x-(x_1+x_s)) ,$$

$$\text{etc.} \qquad (5.10)$$

It should be noted that $Nu_{1b}(x)$ in equation (5.9) corresponds to the continuously welded tube.

To calculate the mean Nusselt number Nu_{bm}, the integration in equation (5.5) was computed using Simpson's One-third Rule. Figure 5.3 shows $Nu_b(x)$ and $Nu_{bm}(x)$ for the arbitrarily chosen case of $\phi_o=\pi/10$, w=60% and N=2, while Figure 5.4 shows $Nu_{bm}(x)$ for $\phi_o=\pi/10$, w=60% and N=8. Because of the discontinuous nature of $Nu_b(x)$, $Nu_{bm}(x)$ in both cases possess abrupt fluctuations. Nonetheless, the fluctuations stabilize downstream and $Nu_{bm}(x)$ approaches an asymptotic

value. In reality, the fluctuations of $Nu_{bm}(x)$ as well as that of the temperature profiles stabilize at a shorter downstream distance than is shown due to conduction in the tube wall [19].

5.4 EFFICIENCY FACTOR FOR VARIOUS SPOT CONFIGURATIONS

The ultimate goal of developing closed form solutions illustrated in the previous two sections was to predict the lower limit of the collector efficiency factor F' of a spot-welded tube. This section presents graphical illustrations of F' for various spot configurations.

Fixing the tube inner radius a to be 4.5 mm, and the Peclet number to be 5060,[12] the tube length of 2m corresponds to the dimensionless distance x of 0.088. The Nusselt number averaged over the tube length was found by evaluating $Nu_{bm}(x)$ at x = 0.088. The spot configuration is completely determined by the half-spot angle ϕ_o, welded percentage w of tube length, and the total number N of spots along a tube. This is based on the assumption that spot length and spot spacing are invariant with position for a particular set of ϕ_o, w and N. For a tube spacing W of 0.15 m, the value of $Nu_{bm}(.088)$ was plotted against N in Figure 5.5 for $\phi_o = \pi/10$ (i.e. spot angle = 36°) for various values of w. The corresponding F' was computed and was plotted in Figure 5.6.

---

[12] See Appendix A

As expected, the efficiency factor F' decreases as w decreases, and the decrease is faster when w is small. The more interesting aspect is the increase of F' with N. It can also be observed that increasing N beyond about 40 does not increase F' significantly.

6. DISCUSSION AND CONCLUSIONS

The problem of a series of spots of heat flux has been solved by two independent methods. The analytical method and its results of this problem have been described in Chapter 3. The same problem has been solved using a finite difference formulation with an iterative scheme (Chapter 4). A comparison of the two methods and their results is appropriate.

6.1 DISCUSSION OF ANALYTICAL AND NUMERICAL METHODS

The analytical solution to the "thin" spot-welded tube was obtained by superposing the available solution due to Bhattacharyya and Roy [15]. The energy equation (equ.(3.3)) that was to be solved is linear. Furthermore, the axial boundary condition of this problem assumes a form[13] which is a simple summation of Heaviside unit step functions, shifted and inverted along the x-axis. The solution can therefore be obtained by simply shifting, inverting, and summing up a number of the same solution (the solution to the continuously welded tube whose axial boundary condition consists of a single unit step function).

To calculate the Nusselt numbers for the continuously welded tube using Bhattacharyya and Roy's solution, only the wall temperature $t(1,\phi,x)$ needs to be computed. This is because the bulk mean temperature is simply given by

---

[13] Illustrated in Figure 2.3 and depicted by equation(2.10).

$$t_m(x) = 4x \ .$$

The computation of $t(1,\phi,x)$ involved three infinite series which appeared in equation (3.16) :

(i) $\sum_{m=1}^{\infty} [a_m \cos m\phi)/m]$,

where $a_m = 2\sin(m\phi_o)/(m\phi_o)$;

(ii) $\sum_{s=1}^{\infty} c_{0s} R_{0s}(1,\beta_{0s}) \exp(-\beta_{0s}^2 x)$;

(iii) $\sum_{m=1}^{\infty} \sum_{s=0}^{\infty} [c_{ms} R_{ms}(1,\beta_{ms}) (a_m \cos m\phi) \exp(-\beta_{ms}^2 x)]$.

Convergence of the first series was slow and sometimes uncertain because of the fluctuation of the term $\cos(m\phi)$ with m. Convergence was tested only after 200 terms had been included in the series. Although the same problem also occurred in the third series, the expression in square brackets decayed exponentially with increasing m and s and was insignificant when $m \simeq s > 10$. The number of terms required by the second and third series increased when x was small (i.e. $x < 5 \times 10^{-3}$).

The superposed solution for the spot-welded tube did not increase the computational time significantly once the solution for the continuously welded tube had been stored as a function of x. This was the main advantage of the present method over directly applying Duhamel's superposition formula.

It should be pointed out that the analytical solution is relatively easy computationally for the wall temperature because the eigenvalues and eigenfunctions involved have

been tabulated in Bhattacharyya and Roy's paper, and can be readily used. The temperature distribution inside the tube (i.e. $r<1$) has not been computed because those eigenvalues and eigenfunctions for $r<1$, which require much computation, are not tabulated.

On the other hand, the finite difference method aimed at obtaining the temperature distribution throughout the entire tube volume. The program developed was expensive to run in terms of CPU time and memory space required. This is because the boundary condition involves variation in all three dimensions. The grid spacing had to be small and as a result the number of nodes involved was very large (M_x=400, M_r=10, and M_ϕ=20 for a 2m tube).

Computing the Nusselt numbers by definition (as in equations (3.8) and (3.10)) and comparing with their analytical counterparts offered a check to the correctness of the numerical results, since the temperature in the entire volume was involved in the expression of the bulk mean temperature t_m. A picture of the internal distribution of temperature increased the understanding of the 3-dimensional heat transfer occurring inside the fluid. This understanding was not obtained through the analytical solution.

Nevertheless, it is unfair to compare the computing cost required by the two methods. This is because the eigenvalues and eigenfunctions required by the analytical solution were already given and its computational effort

cannot be accounted for.

6.2 RECOMMENDATIONS

If material cost is not an important consideration in designing the flat plate collector, a thick copper tube is recommended for spot welding. Peripheral and axial conduction inside the tube wall allows heat to be transferred into the fluid throughout the entire tube wall (Figure 2.1(i)), instead of through the welding spots alone. It should be noted, however, that a thick tube is more prone to thermal stresses. The mean Nusselt number for this case approaches an upper limit : Nu_m for the uniform wall temperature case. This mean Nusselt no. $Nu_m(.088)$ is tabulated in Shah and London [3] to be 4.776, and corresponds to an efficiency factor F' of 0.883. The actual value of F' is, of course, lower and depends on the total amount of welding being done, as well as the thickness and conductivity of the tube wall.

If a low material cost is desired and the tube wall has to be thin and non-conductive, attention should be paid to the welding spot configuration. When $\gamma/L \leq 0.0001$ for $R_w \geq 2\times10^{-7}$, or when $\gamma/L \leq 0.001$ for $R_w \geq 10^{-5}$, the heat transfer from the fin to the fluid can be thought of as being restricted to the passage provided by the welding spots (Figure 2.1(ii)). The mean Nusselt no. based on bond temperature Nu_{bm} and the efficiency factor F' for this case approach the lower limits given in Figures 5.5 and 5.6,

respectively. The actual value is higher and increases with the increase of (γ/LR_w). The efficiency factor F' is also a strong function of the tube spacing, W, as illustrated in Figures 6.1 and 6.2, where the spot angle have been kept at $\phi_o=\pi/10$.

In any case, spot welding should be done over a large percentage of the tube length and of the circumference. This becomes more important when the tube is thin and non-conductive. This, of course, has to be weighed against the cost of welding. Moreover, spot welding should be done over a large number of closely separated, short spots instead of a small number of widely separated, long spots. The total number of spots should be over 40 per tube (for a typical tube length of 2m). This consideration, important for the thin and non-conductive tube, is to be taken against the controllability of the welding mechanism, usually an industrial robot.

Finally, it should be pointed out that the spot configuration is just one factor determining the efficiency of the spot-welded solar collector. Other parameters, including overall heat transfer coefficient U_L, plate thickness, tube spacing and bond width, etc, affect the spot-welded collector as well as the conventionally welded collector.

6.3 CONCLUSIONS

The objectives of the present work have been achieved. Two ideal models for the heat transfer process inside the spot-welded collector tube were set up in which the boundary conditions could be formulated mathematically. Attention was given to the thin and non-conductive tube, results for which corresponded to the lower limit of performance.

An understanding of the detailed heat transfer phenomenon was obtained through the finite difference solution of the energy equation, which described the temperature distribution inside the entire tube volume. The effect on collector efficiency factor due to spots of heat input was investigated using the analytical solution. This analytical solution was obtained by superposing existing solution available in the literature. The technique of superposition was demonstrated to be of great usefulness in this kind of linear problems. For the thin and non-conductive tube, an interesting finding was that distributing a given amount of welding over a large number of short spots resulted in a higher efficiency factor.

REFERENCES

1. J.A. Duffie and W.A. Beckman : "Solar Engineering of Thermal Processes", John Wiley & Sons, New York. (1980)

2. A. Whillier : "Thermal Resistance of the Tube-Plate Bond in Solar Heat Collectors", **Solar Energy** Vol.8, No.3, pp95-98. (1964)

3. R.K. Shah and A.L. London : "Laminar Flow Forced Convection In Ducts", **Advances in Heat Transfer : Supp.1**, Academic Press. (1978)

4. W.M. Kays and M.E. Crawford : "Convective Heat and Mass Transfer", McGraw Hill. (1966)

5. L. Graetz : "On the Thermal Conductivity of Liquids", Part 1, **Ann. Phys. Chem.** Vol.18, pp79-94. (1883)

6. T.B. Drew : "Mathematical Attacks On Forced Convection Problems : A Review", **Trans. Am.Inst.Chem.Eng.** Vol.26, pp26-80. (1931)

7. G.M. Brown : "Heat or Mass Transfer in a Fluid in Laminar Flow in a Circular or Flat Conduit", **Am.Inst.Chem.Eng. Journal** Vol.6, pp179-183. (1960)

8. J.R. Sellars, M. Tribus and J.S. Klein : "Heat Transfer to Laminar Flow in a Round Tube or Flat Conduit - the Graetz Problem Extended", **Trans. ASME** Vol.78, pp441-448. (1956)

9. M.A. Leveque : "Les lois de la transmission de chaleur par convection", **Ann.Mines.Mem., Ser.12** Vol.13, pp201-299,305-312,381-415. (1928)

10. A.McD. Mercer : "The Growth of the Thermal Boundary Layer at the Inlet to a Circular Tube", **App. Sci. Res., Sect.A** Vol.9, pp450-456. (1960)

11. P.M. Worsoe-Schmidt : "Heat Transfer in the Thermal Entrance Region of Circular Tubes and Annular Passages with Fully Developed Laminar Flow", **Int.J. Heat Mass Transfer** Vol.10, pp541-551. (1967)

12. J. Newman : "Extension of the Leveque Solution", **J. Heat Transfer, Trans. ASME** Vol.90, pp361-363. (1969)

13. U. Grigull and H. Tratz : "Thermischer einlauf in ausgebildeter laminarer rohrstromung", **Int. J. Heat Mass Transfer** Vol.8, pp669-678. (1965)

14. W.C. Reynolds: "Heat Transfer to Fully Developed Laminar Flow in a Circular Tube with Arbitrary Circumferential Heat Flux", **J. Heat Transfer, Trans. ASME** Vol.82, pp108-111. (1960)

15. T.K. Bhattacharyya and D.N. Roy : "Laminar Heat Transfer in a Round Tube with Variable Circumferential or Arbitrary Wall Heat Flux", **Int.J. Heat Mass Transfer**, Vol.13, pp1057-1060. (1963)

16. A.V. Luikov, V.A. Alekasashenko and A.A. Alekasashenko : "Analytical Methods of Solution of Conjugated Problems in Convective Heat Transfer", **Int. J. Heat Mass Transfer**, Vol.14, pp1047-1056. (1971)

17. S. Mori, M. Sakakibara and A. Tanimoto : "Steady Heat Transfer to Laminar Flow in a Circular Tube with Conduction in the Tube Wall", **Heat Transfer - Japanese Research** Vol.3(2), pp37-46. (1974)

18. M. Faghri, E.M. Sparrow : "Simultaneous Wall and Fluid Axial Conduction in Laminar Pipe-flow Heat Transfer", **J. Heat Transfer, Trans. ASME** Vol.102, pp58-63. (1980)

19. G.S. Barozzi and G. Pagliarini : "Conjugated Heat Transfer in a Circular Duct with Uniform and Non-uniform Wall Thickness", **Heat and Technology** Vol.2, pp72-89. (1984)

20. L.C. Burmeister : "Convective Heat Transfer", Wiley Interscience. (1983)

21. C.J. Hsu : "An Exact Analysis of Low Peclet number Thermal Entry Region Heat Transfer in Transversely Non-uniform Velocity Fields", **Am.Inst.Chem.Eng. Journal**, Vol.17, No.3, pp732-740. (1971)

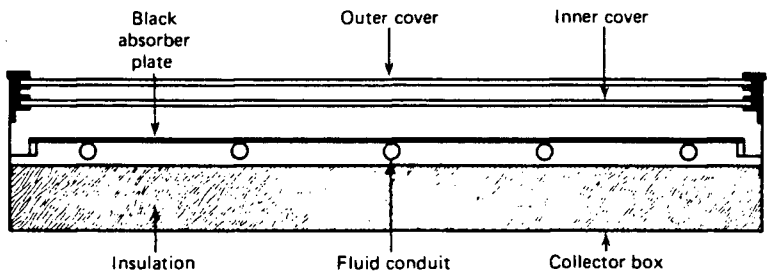

FIG 1.1 Cross section of a basic flat plate solar collector

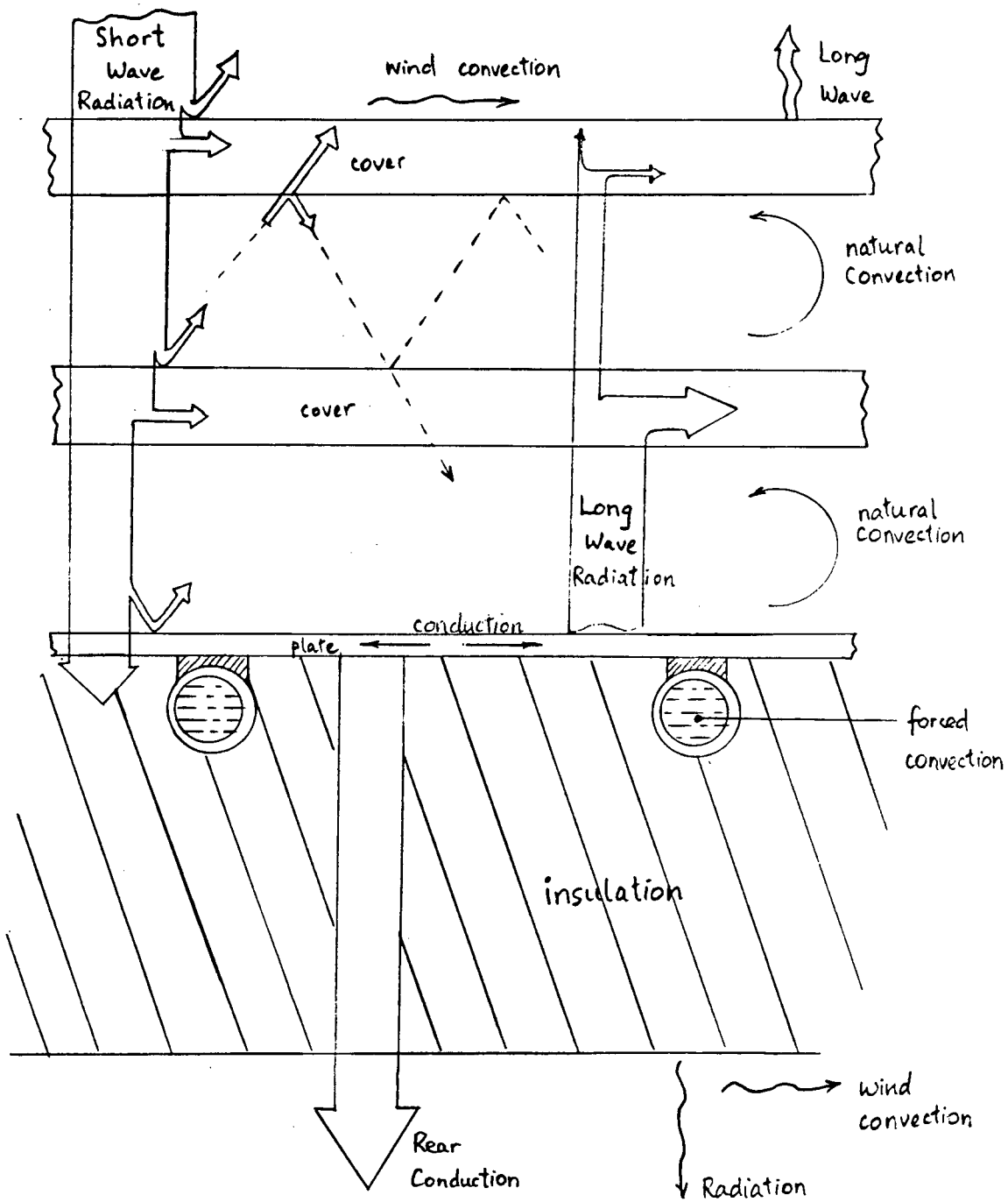

FIG. 1.2. Energy flow in an operating solar collector.

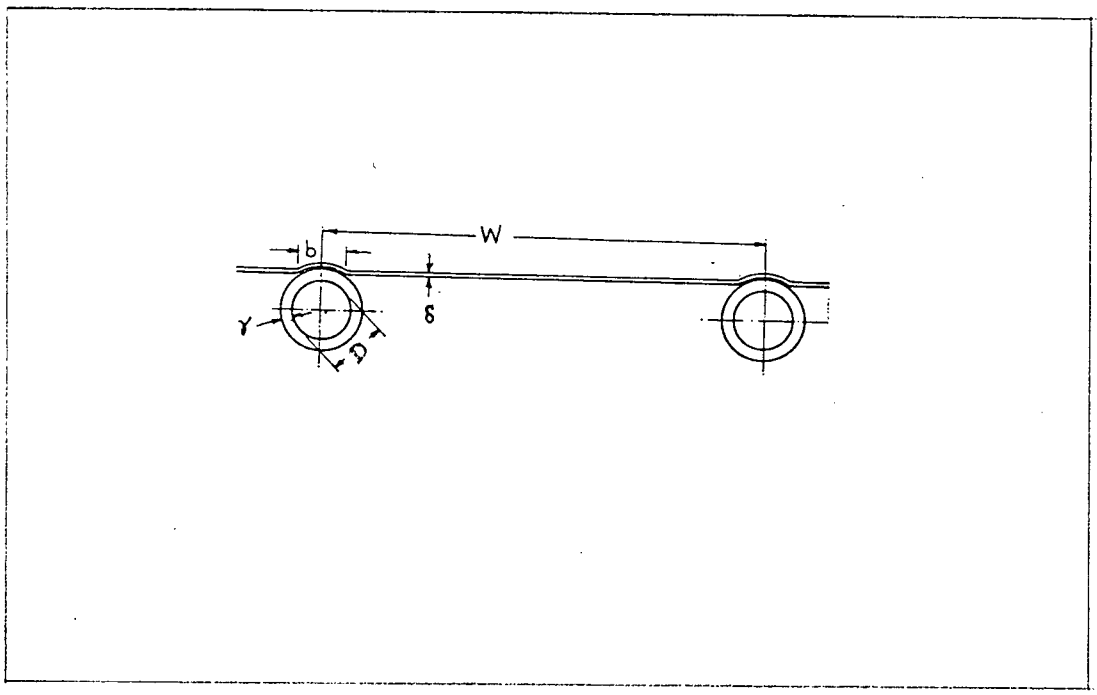

FIG 1.3 Cross section of plate and tube arrangement

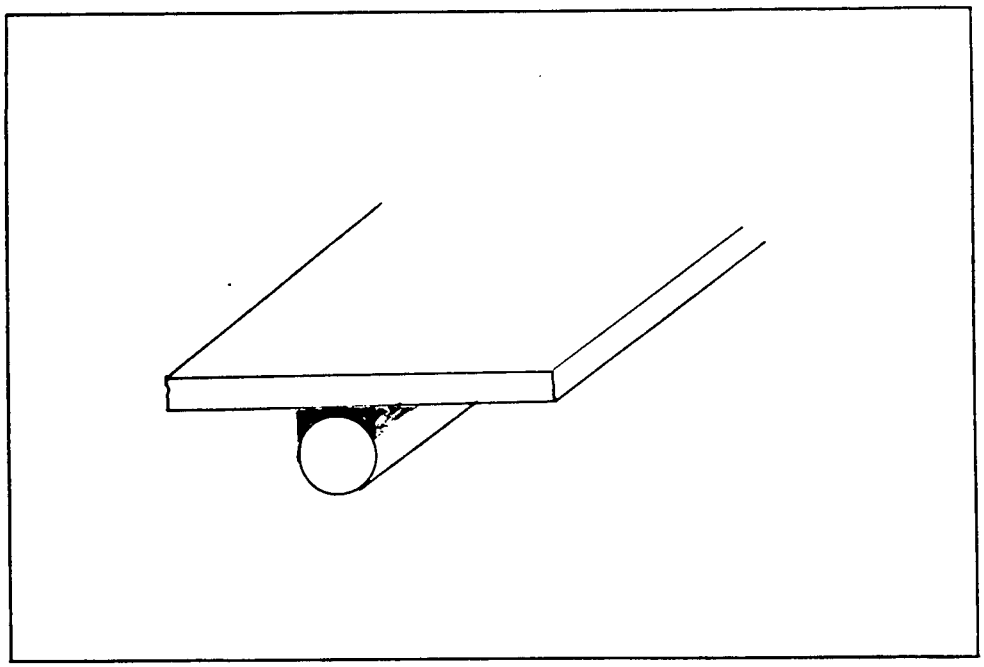

(i)Tube is soldered throughout its length onto plate

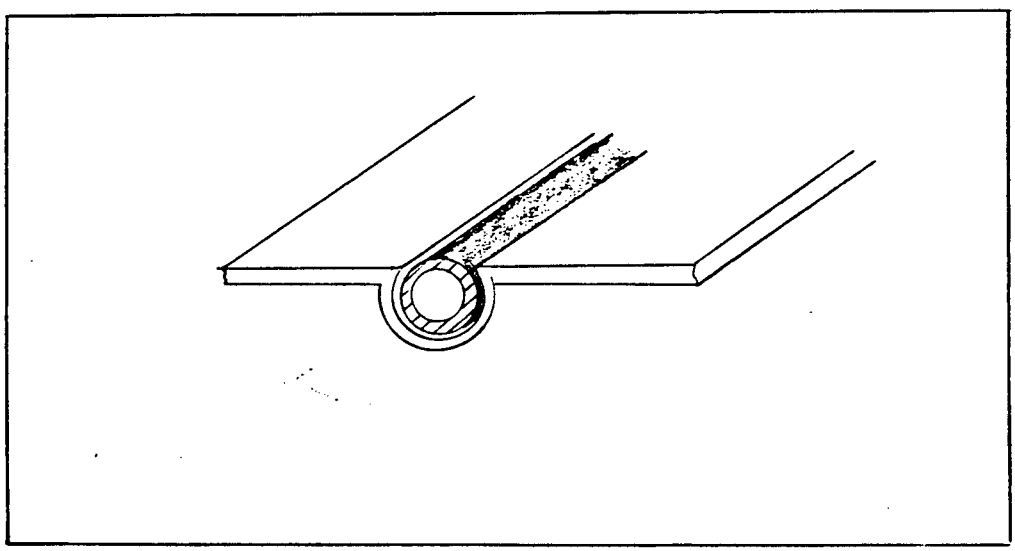

(ii)Tube embedded in trough formed by plate

FIG. 1.4. Common ways of plate-tube bonding.

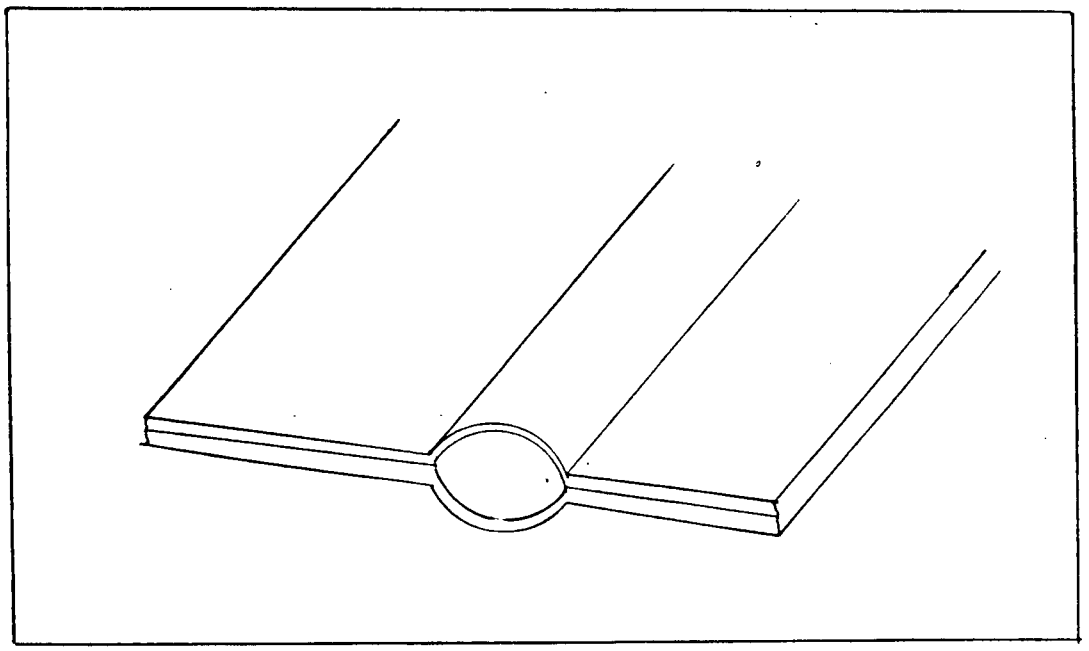

(iii)Plate includes conduit within itself

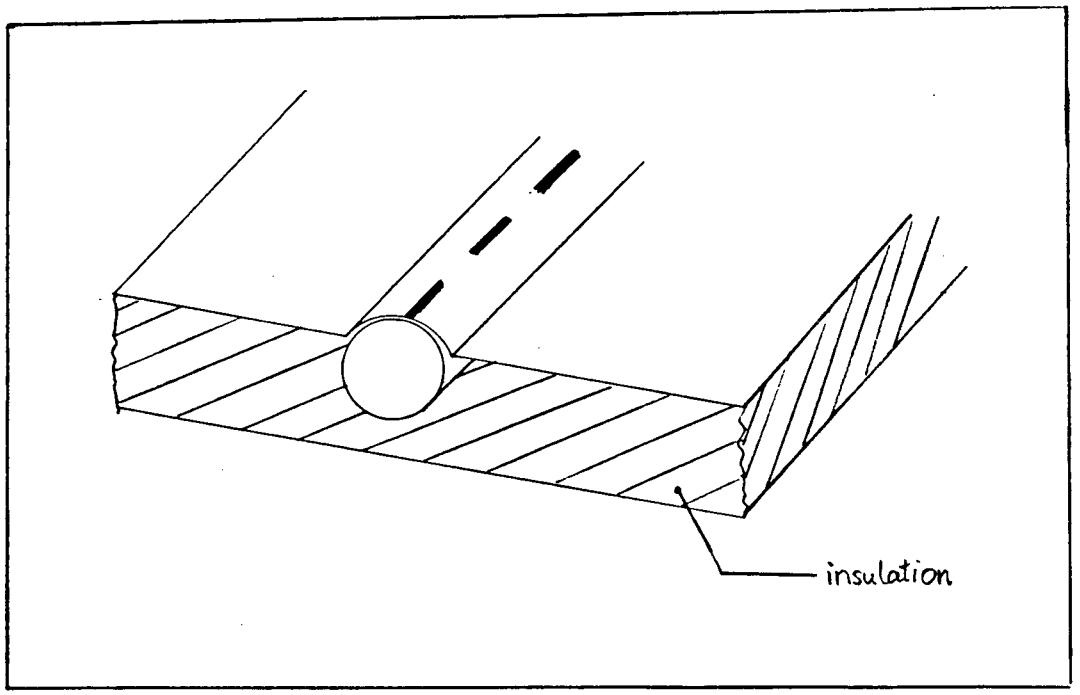

(iv)Tube is welded onto plate at separated spots

FIG 1.4 Common ways of plate-tube bonding

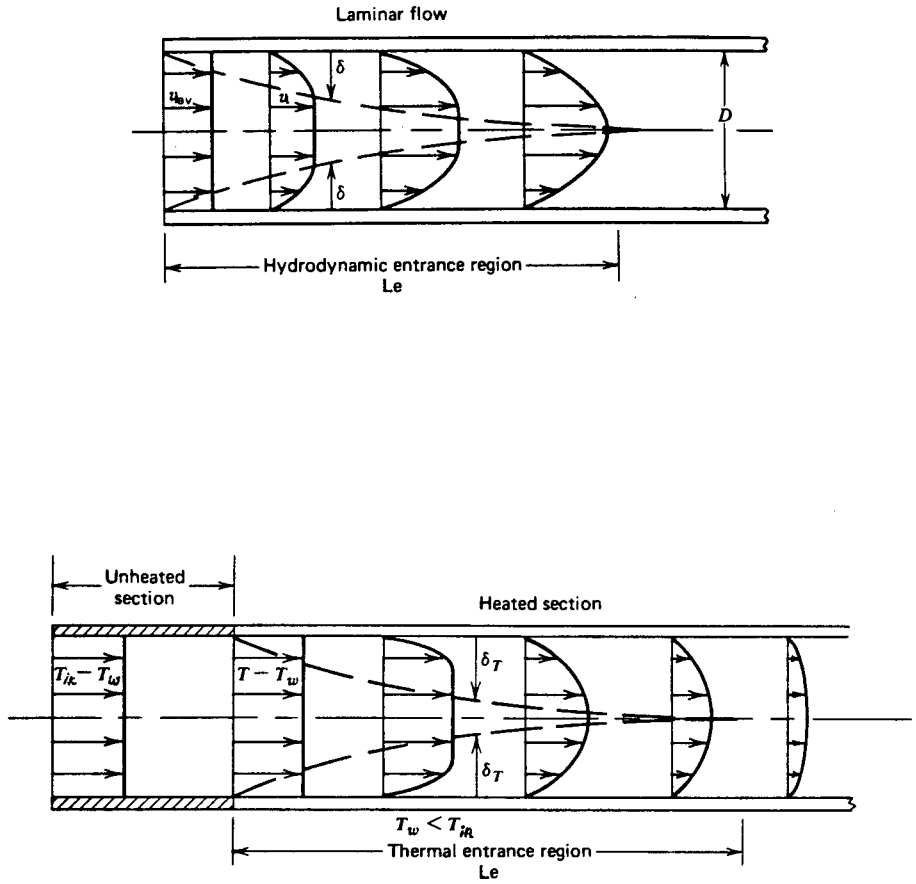

FIG 1.5 Hydrodynamic and thermal entry lengths

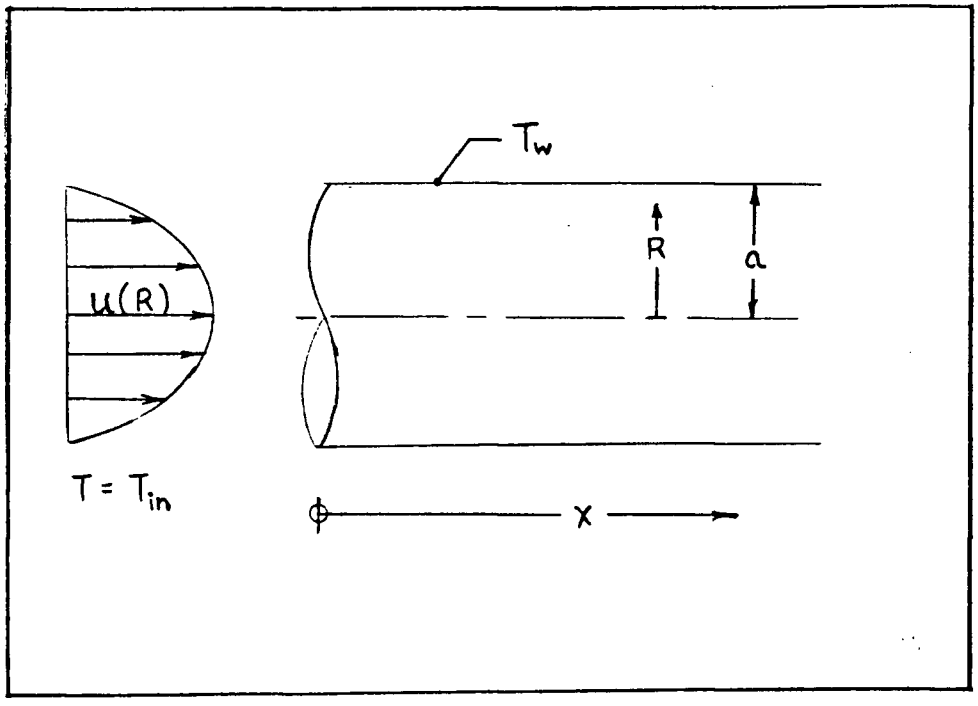

FIG 1.6 Physical situation of Graetz problem

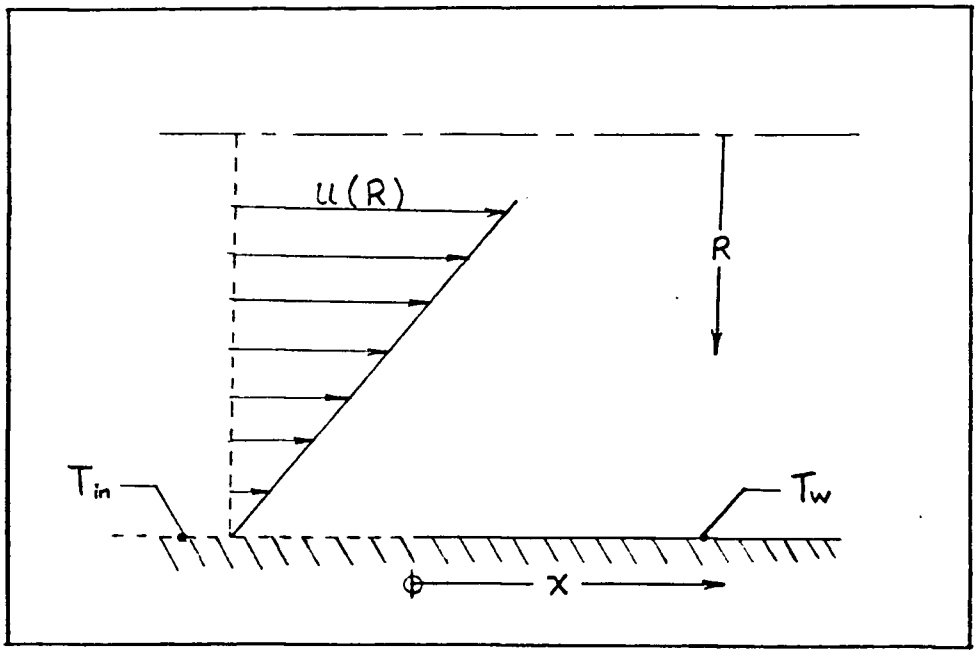

FIG 1.7 Linear velocity profile assumed in Leveque method

Designation	Description	Applications
Ⓣ	Constant wall temperature peripherally as well as axially	Condensers, evaporators, automotive radiators (at high flows), with negligible wall thermal resistance
(T3)	Constant axial wall temperature with finite normal wall thermal resistance	Same as those for Ⓣ with finite wall thermal resistance
(T4)	Nonlinear radiant-flux boundary condition	Radiators in space power systems, high-temperature liquid-metal facilities, high-temperature gas flow systems
(H1)	Constant axial wall heat flux with constant peripheral wall temperature	Same as those for (H4) for highly conductive materials
(H2)	Constant axial wall heat flux with uniform peripheral wall heat flux	Same as those for (H4) for very low conductive materials with the duct having uniform wall thickness
(H3)	Constant axial wall heat flux with finite normal wall thermal resistance	Same as those for (H4) with finite normal wall thermal resistance and negligible peripheral wall heat conduction
(H4)	Constant axial wall heat flux with finite peripheral wall heat conduction	Electric resistance heating, nuclear heating, gas turbine regenerator, counterflow heat exchanger with $C_{min}, C_{max} \simeq 1$, all with negligible normal wall thermal resistance
(H5)	Exponential axial wall heat flux	Parallel and counterflow heat exchangers
(Δt)	Constant axial wall to fluid bulk temperature difference	Gas turbine regenerator

Table 2.1 Thermal boundary conditions for developed and developing flows through singly connected ducts

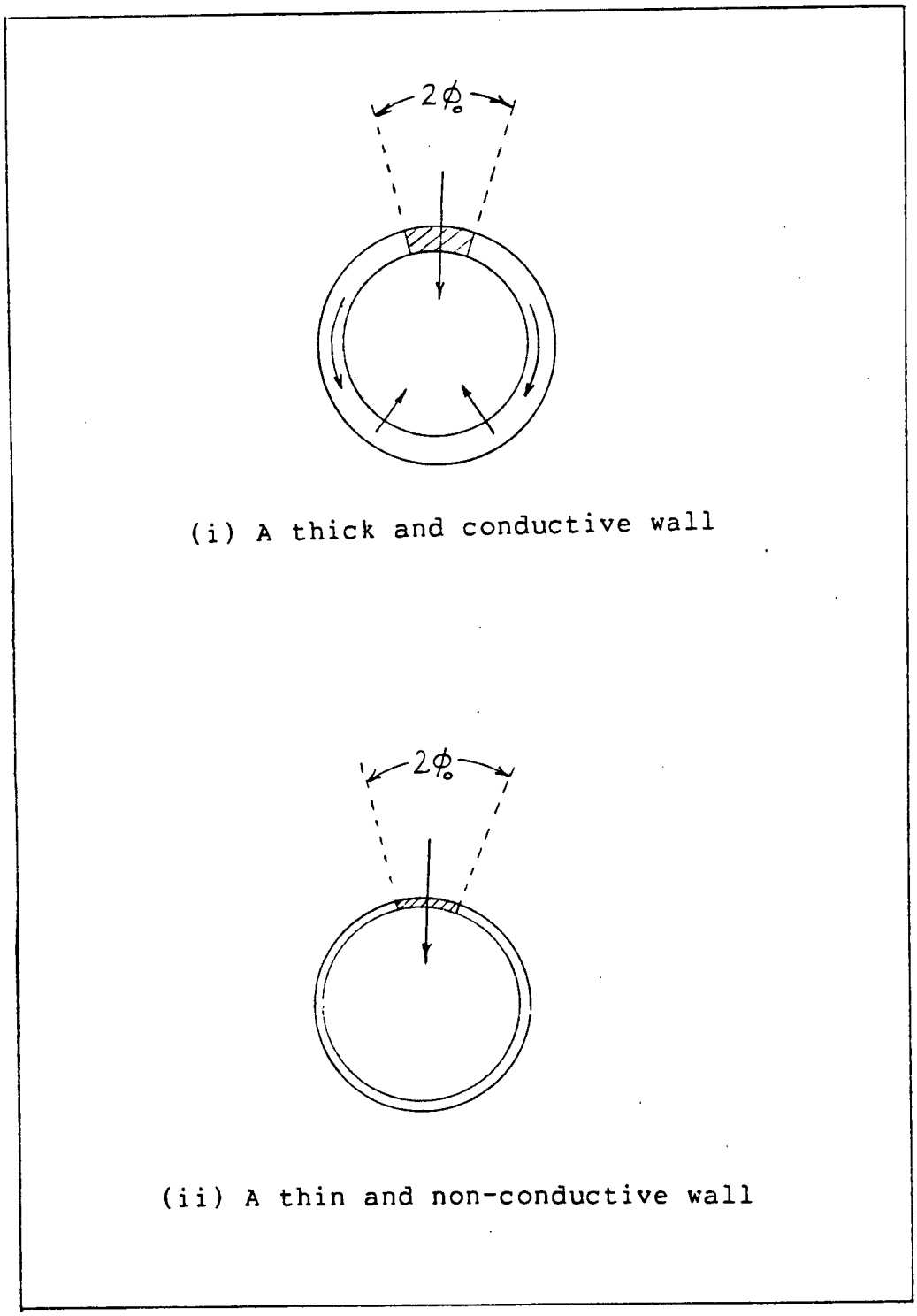

FIG 2.1 Two extreme cases of thermal boundary conditions

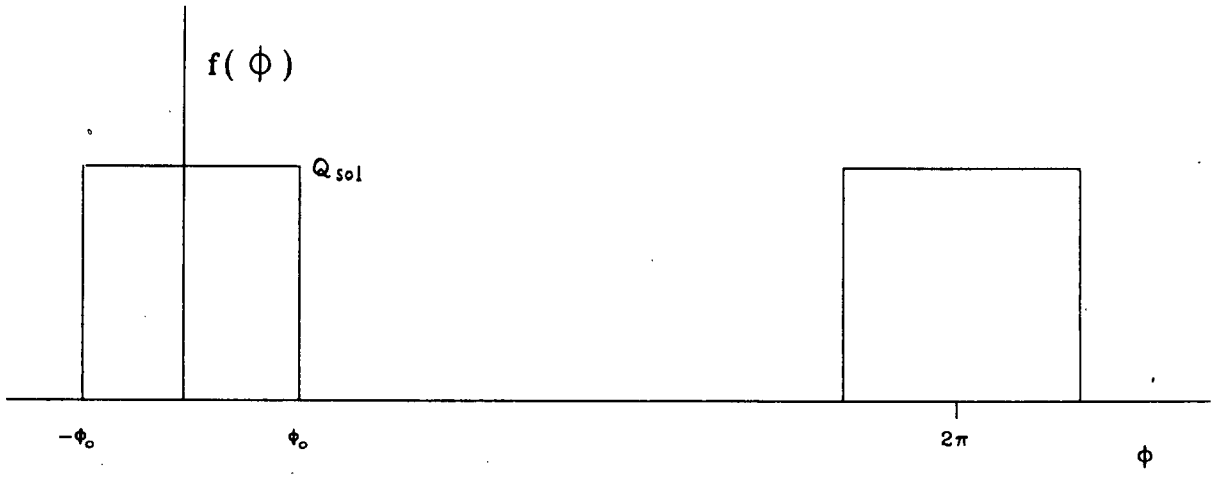

FIG 2.2 Peripheral distribution of wall heat flux

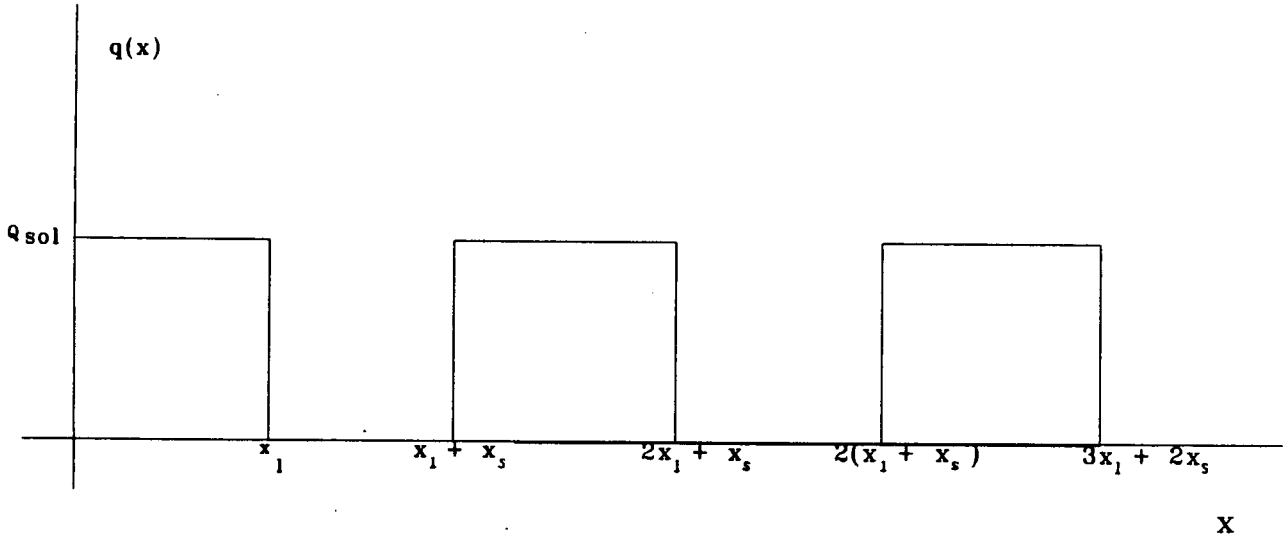

FIG 2.3 Axial distribution of wall heat flux

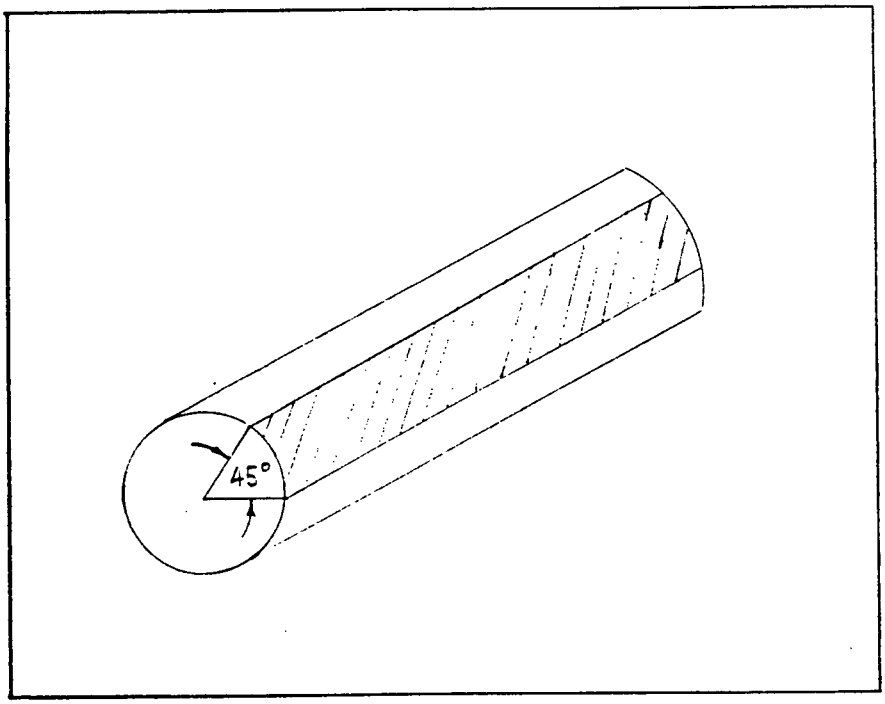

FIG 3.1 Continuously welded tube with spot angle of 45°

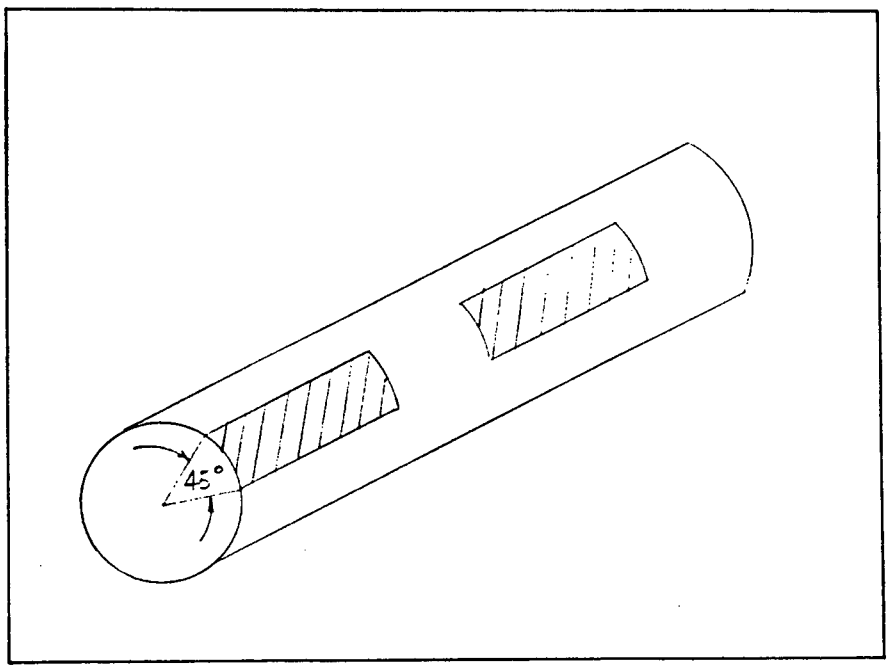

FIG 3.2 Spot welded tube with 2 spots occupying 60% of its length

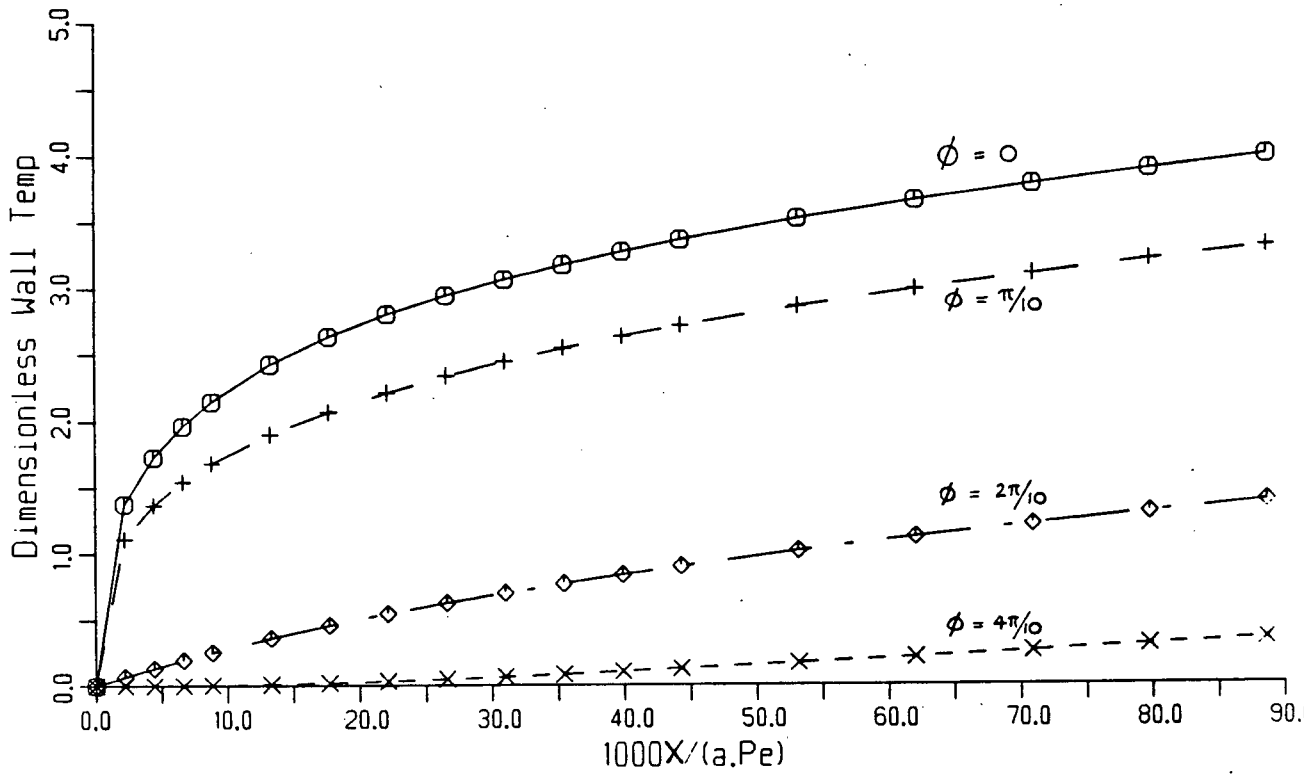

FIG. 3.3 Dimensionless wall temperature of continuously welded tube with spot angle 45° versus dimensionless axial distance 1000x=1000X/a·Pe.

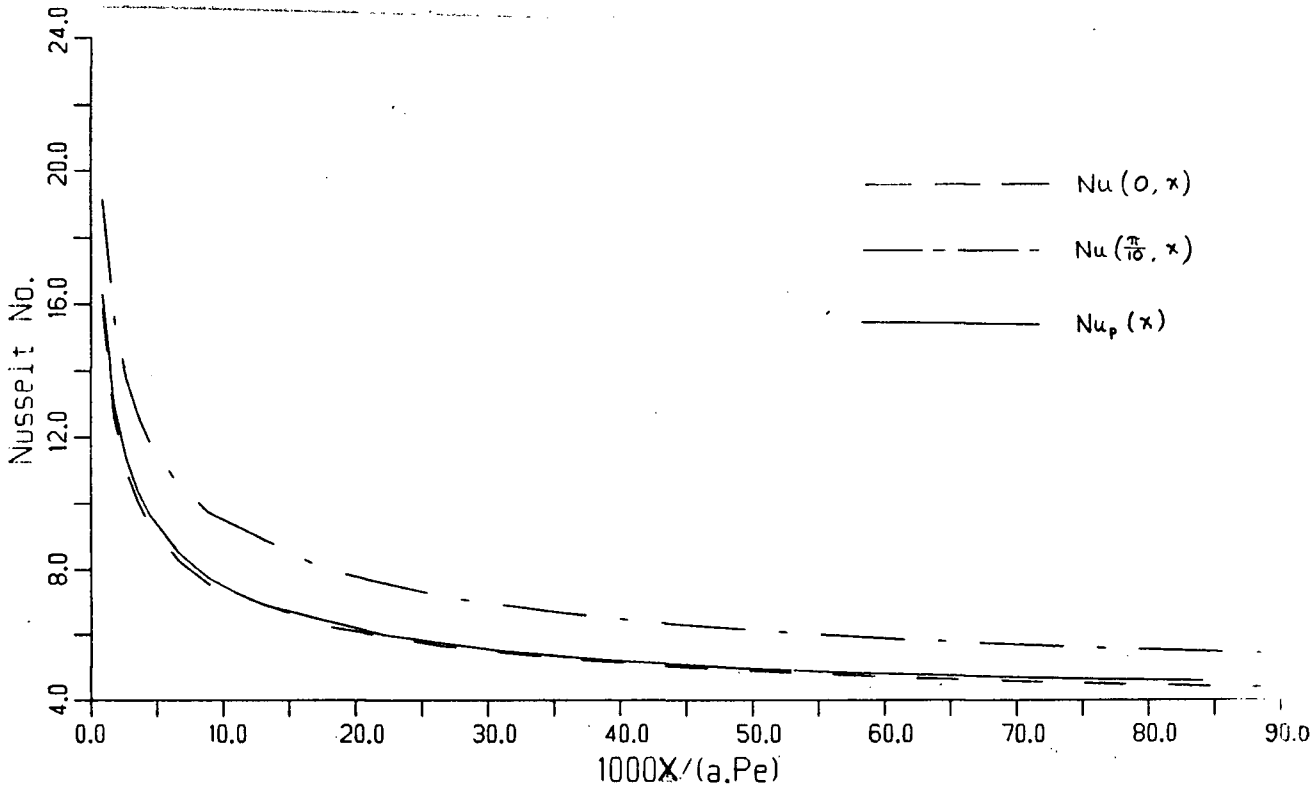

FIG. 3.4. Local Nusselt no. Nu and peripheral average Nusselt no. Nu_p of continuously welded tube versus dimensionless axial distance 1000x=1000X/a·Pe.

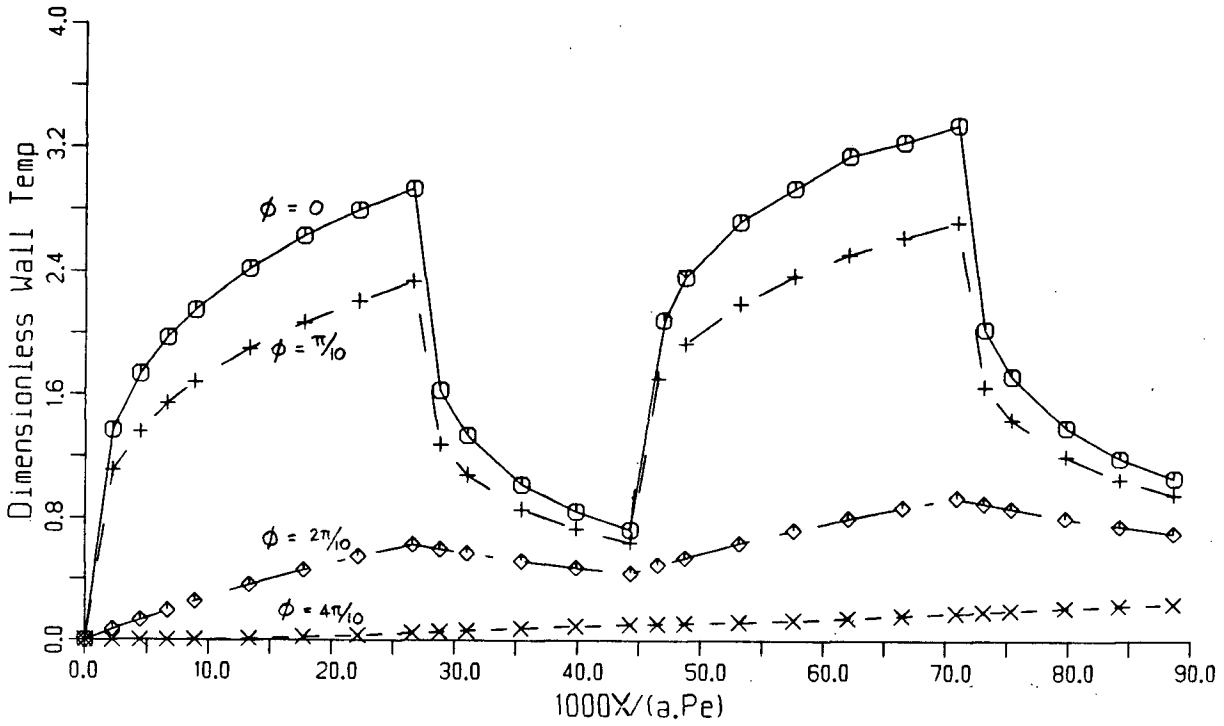

FIG. 3.5. Dimensionless wall temperature versus dimensionless axial distance 1000x = 1000X/a·Pe of a spot welded tube with 2 spots occupying 60% of its length, spot angle 45°.

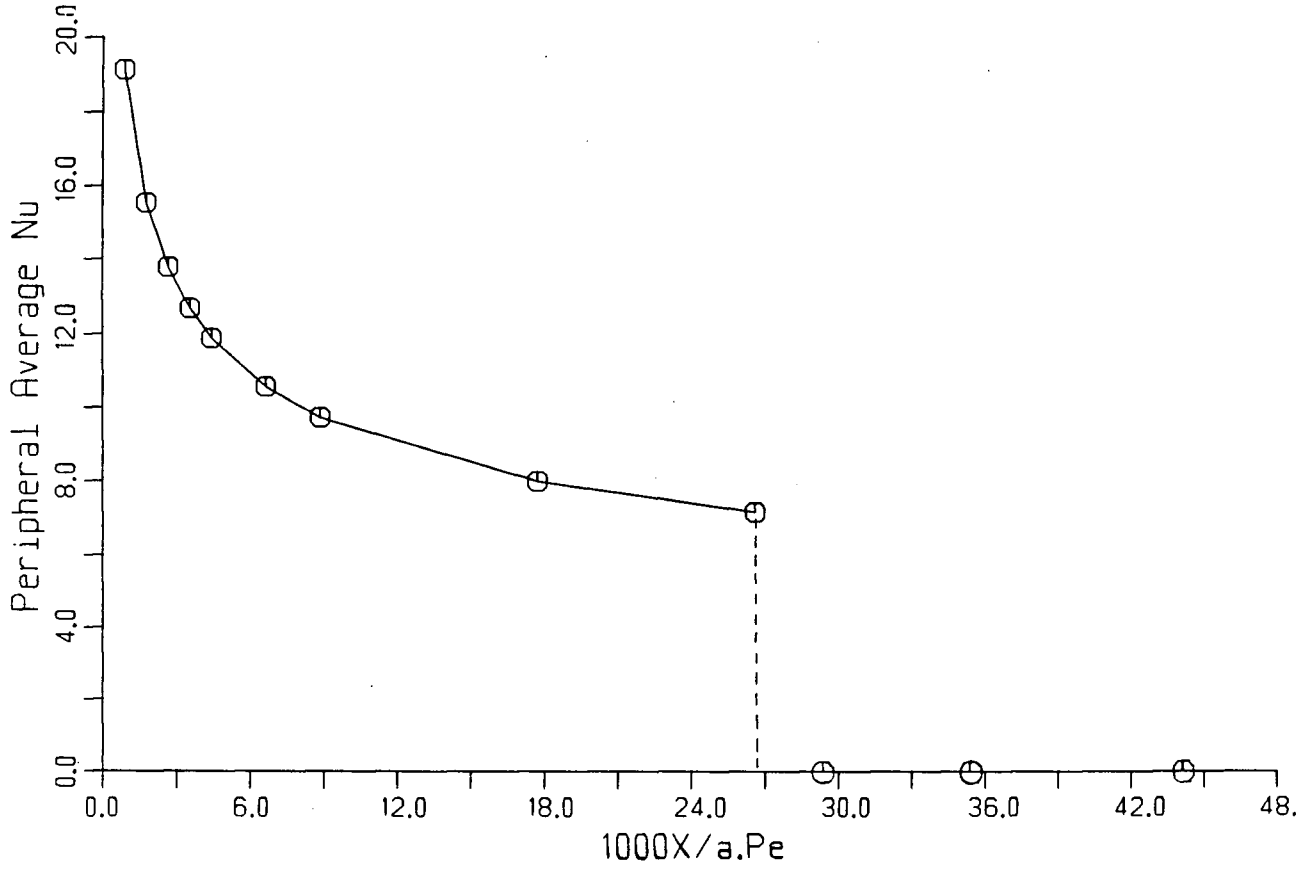

FIG. 3.6(i). Peripheral average Nusselt no. Nu_p versus dimensionless axial distance 1000x=1000X/a·Pe for a spot-welded tube with a single spot occupying 60% of its length, spot angle 45°.

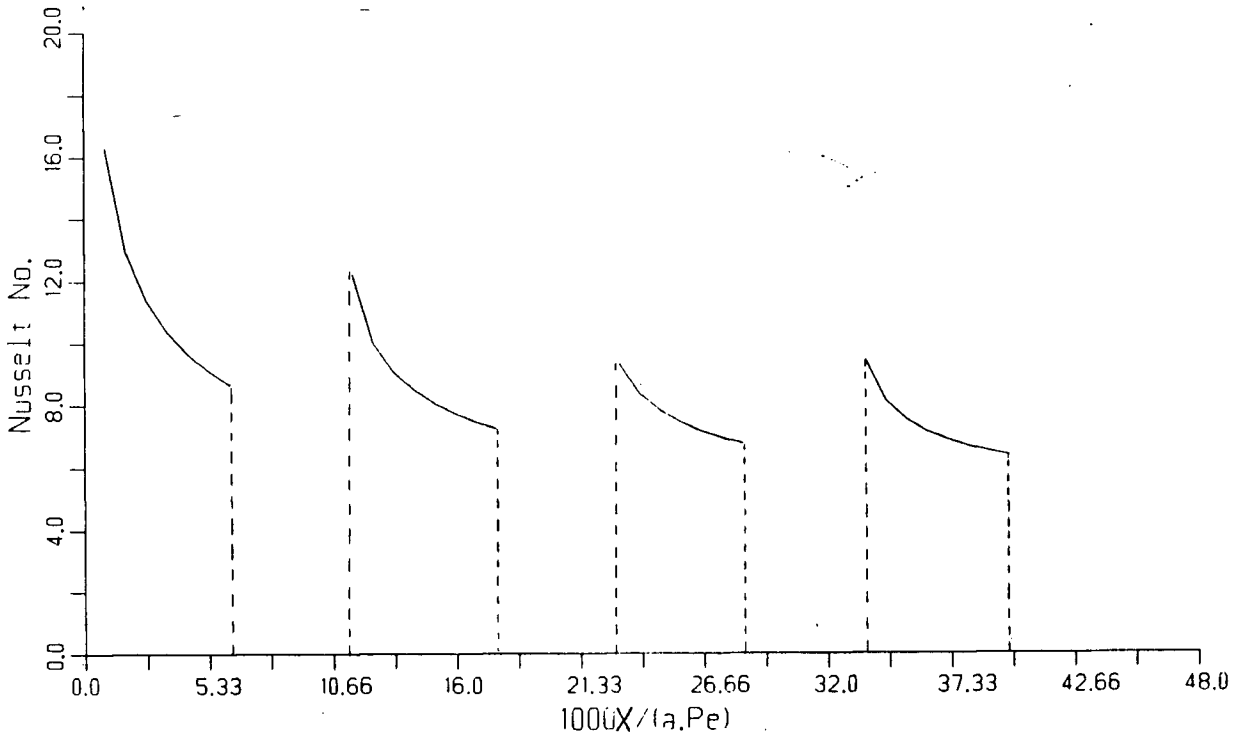

FIG. 3.6(ii). Peripheral average Nusselt no. Nu_p versus dimensionless axial distance $1000x=1000X/\bar{a}\cdot Pe$ for a spot-welded tube with 4 spots occupying 60% of its length, spot angle 45°.

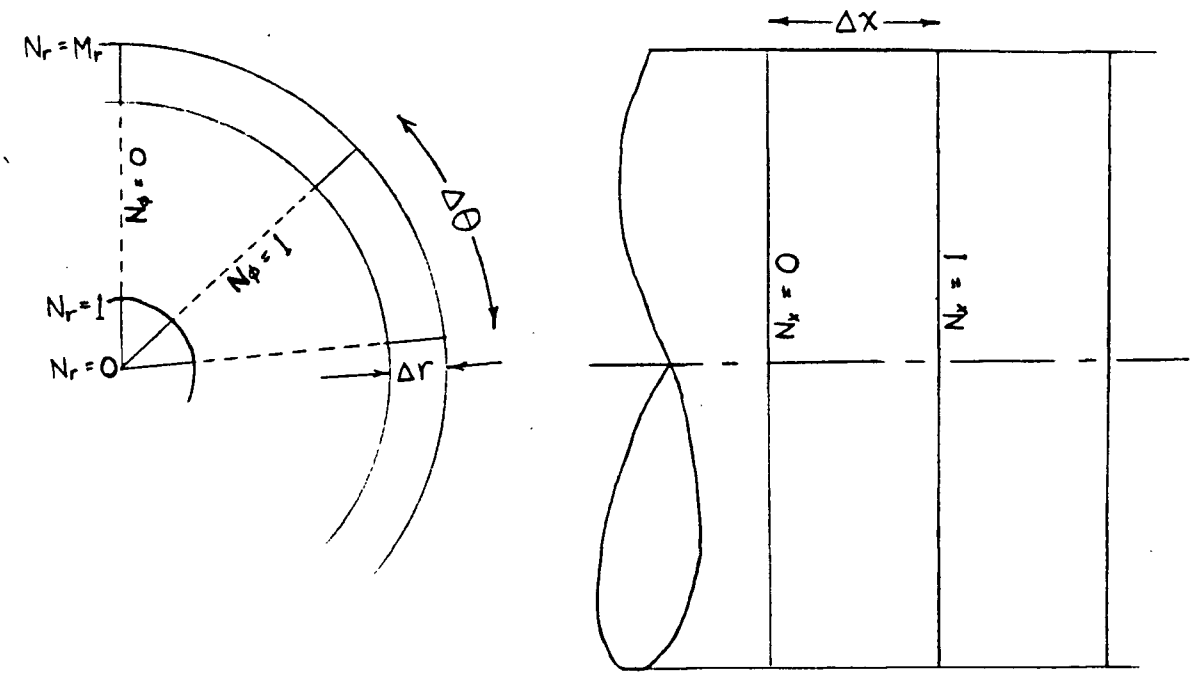

FIG 4.1 Grid division of tube volume.

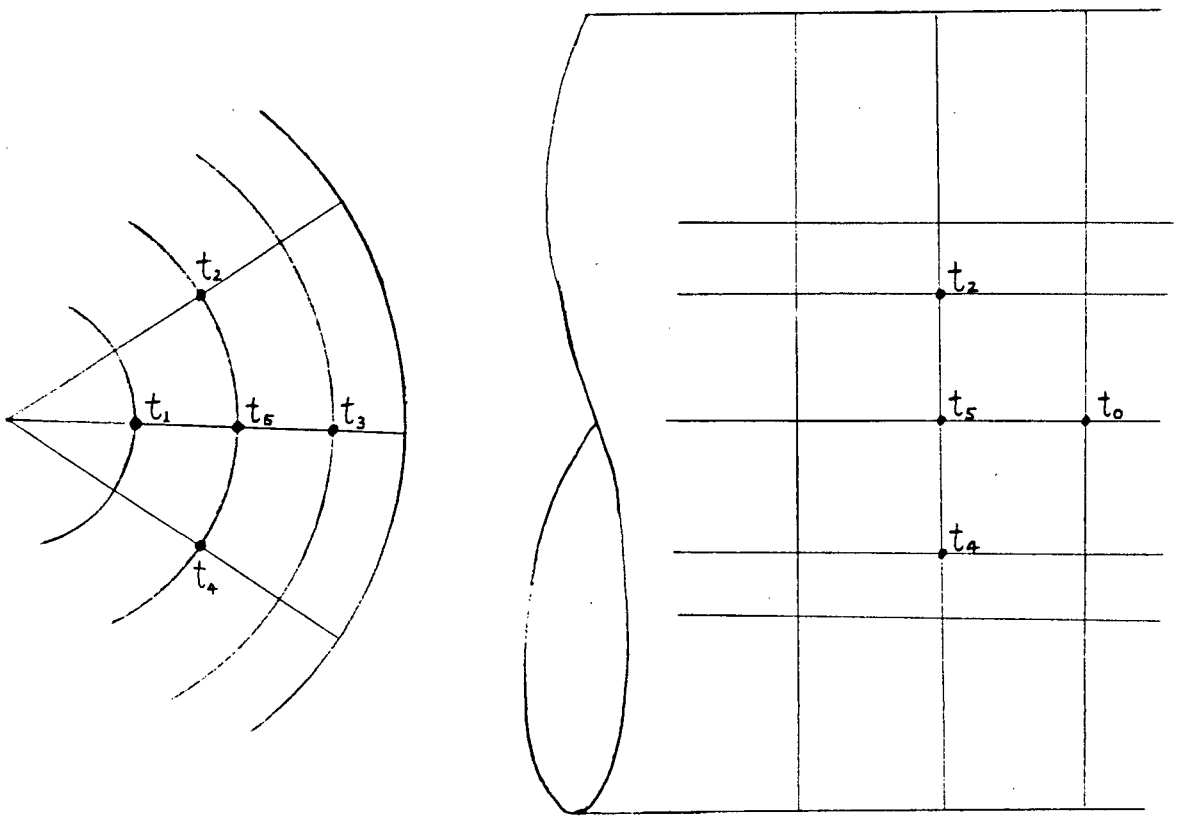

FIG 4.2 Node positions appeared in finite difference energy equation

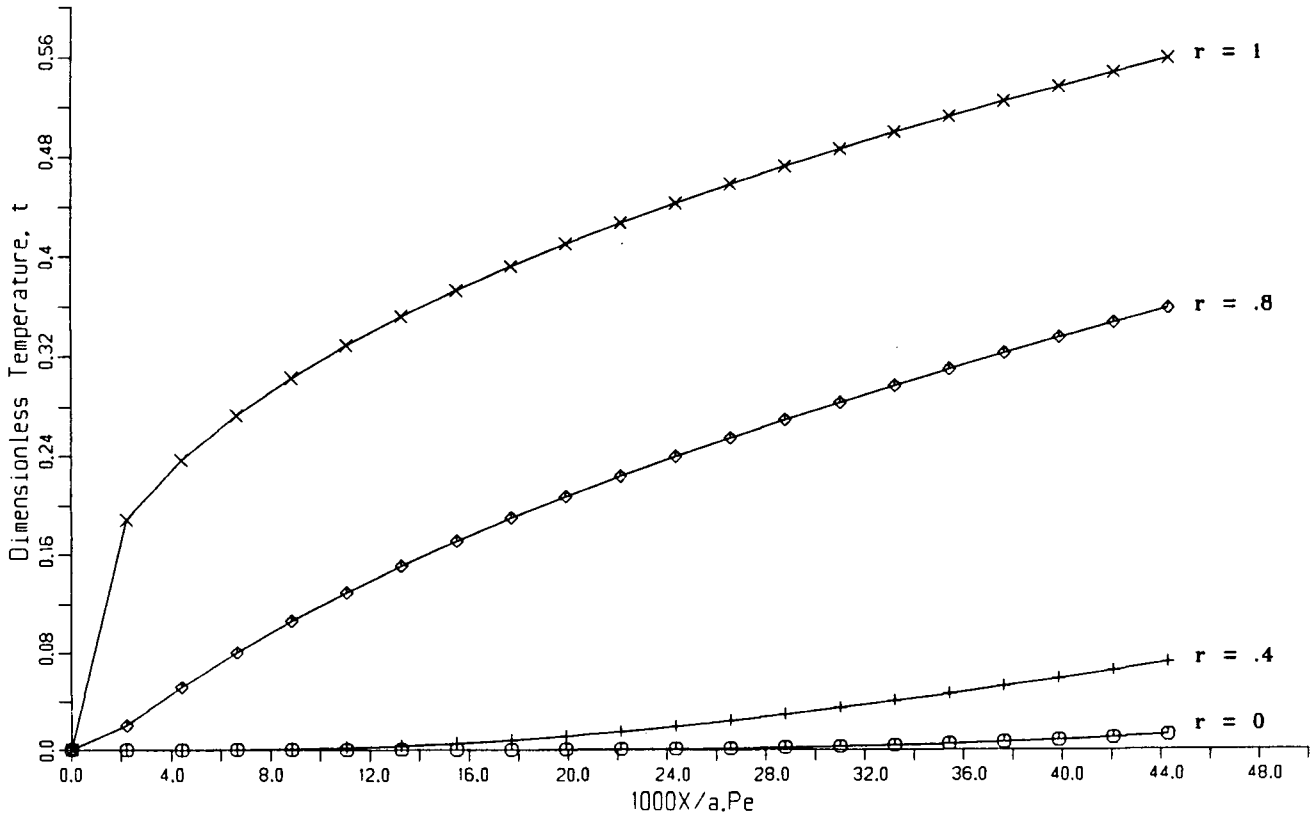

FIG. 4.3. Dimensionless temperature t of a uniformly heated tube versus dimensionless axial distance 1000x = 1000X/a·Pe at various radial distances : finite difference results.

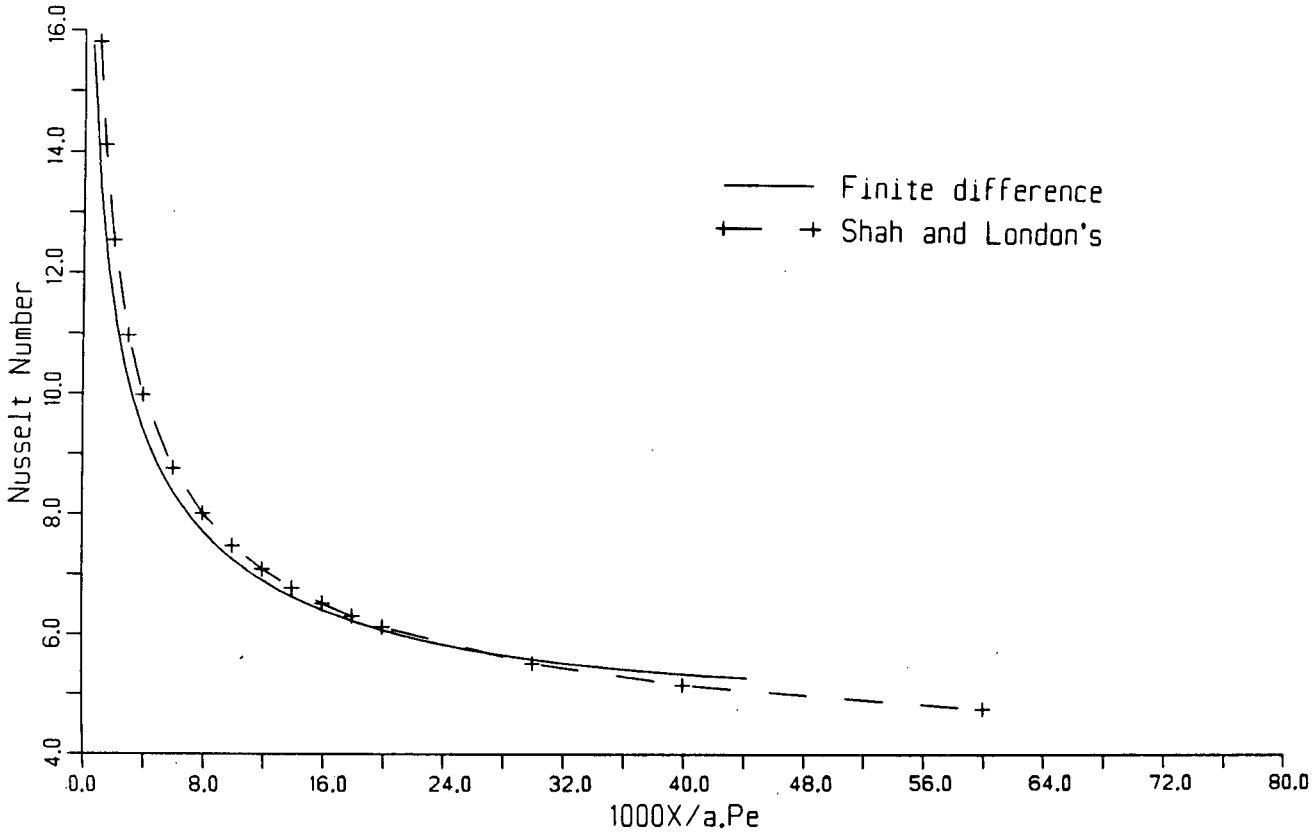

FIG. 4.4. Local Nusselt no. Nu of a uniformly heated tube versus dimensionless axial distance 1000x = 1000X/a·Pe : finite difference results.

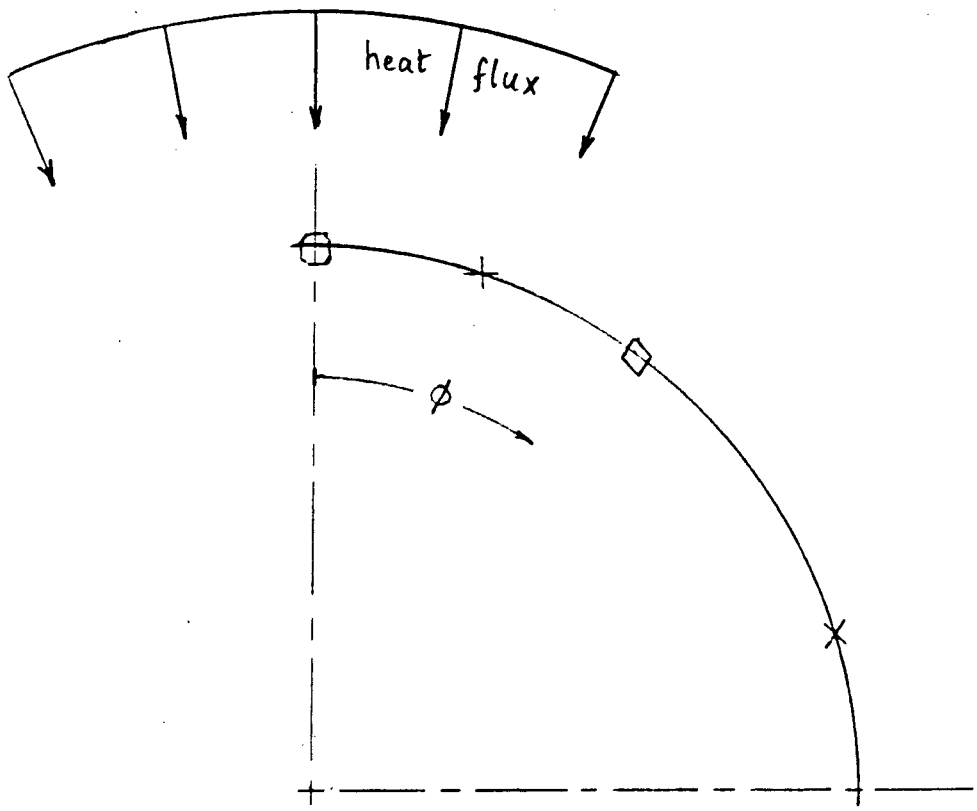

FIG. 4.5. Angular positions represented by various curves in Figures 4.6 - 4.9.

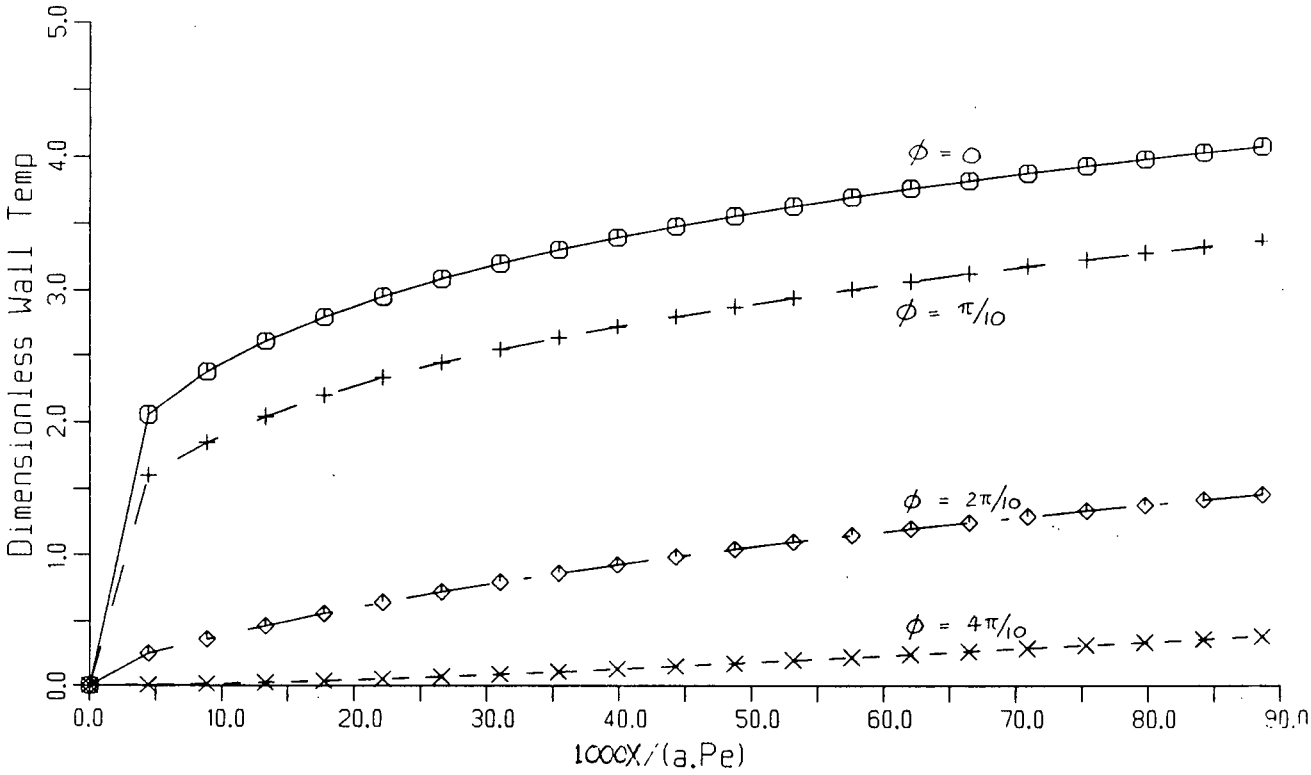

FIG. 4.6. Dimensionless wall temperature versus dimensionless axial distance 1000x = 1000X/a·Pe : finite difference results for a continuously welded tube with spot angle 45°.

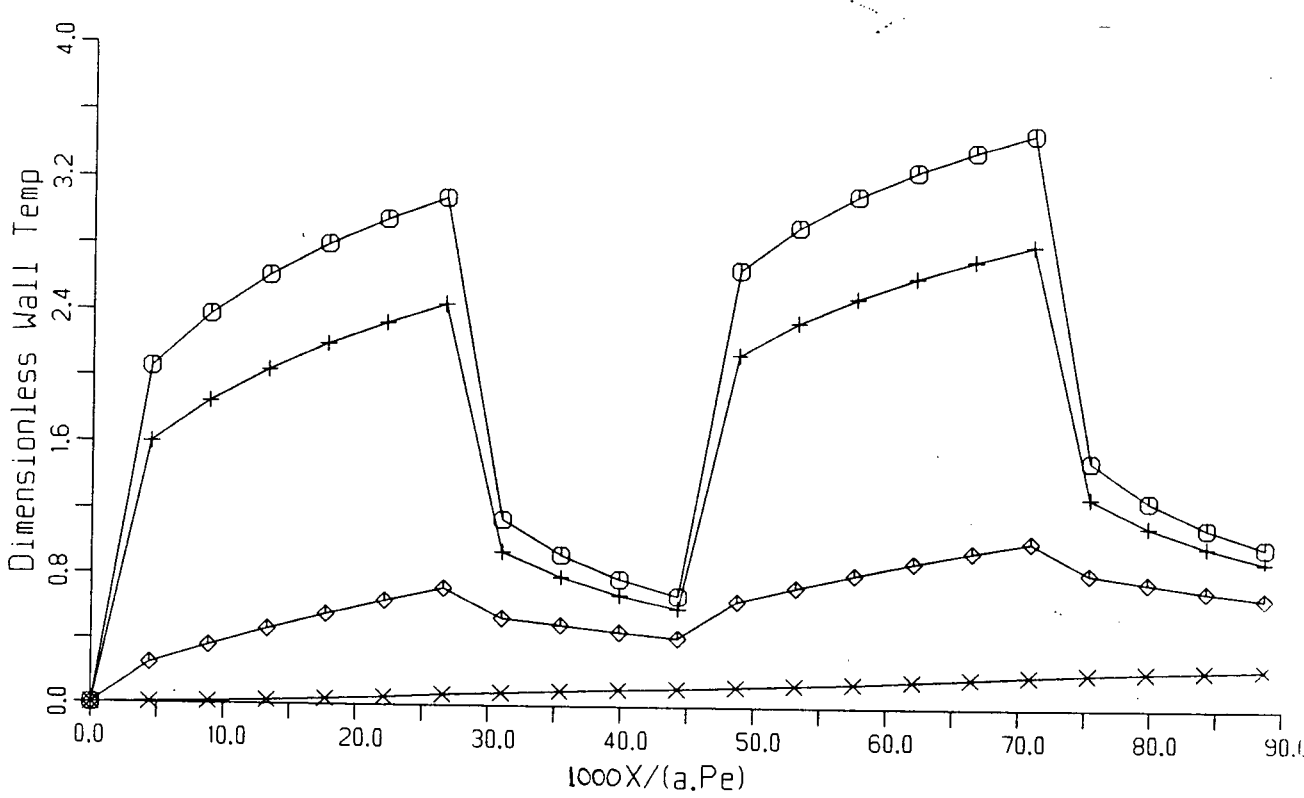

FIG. 4.7. Dimensionless wall temperature versus dimensionless axial distance 1000x = 1000X/a·Pe : finite difference results for a spot-welded tube with 2 spots occupying 60% of its length, spot angle 45°.

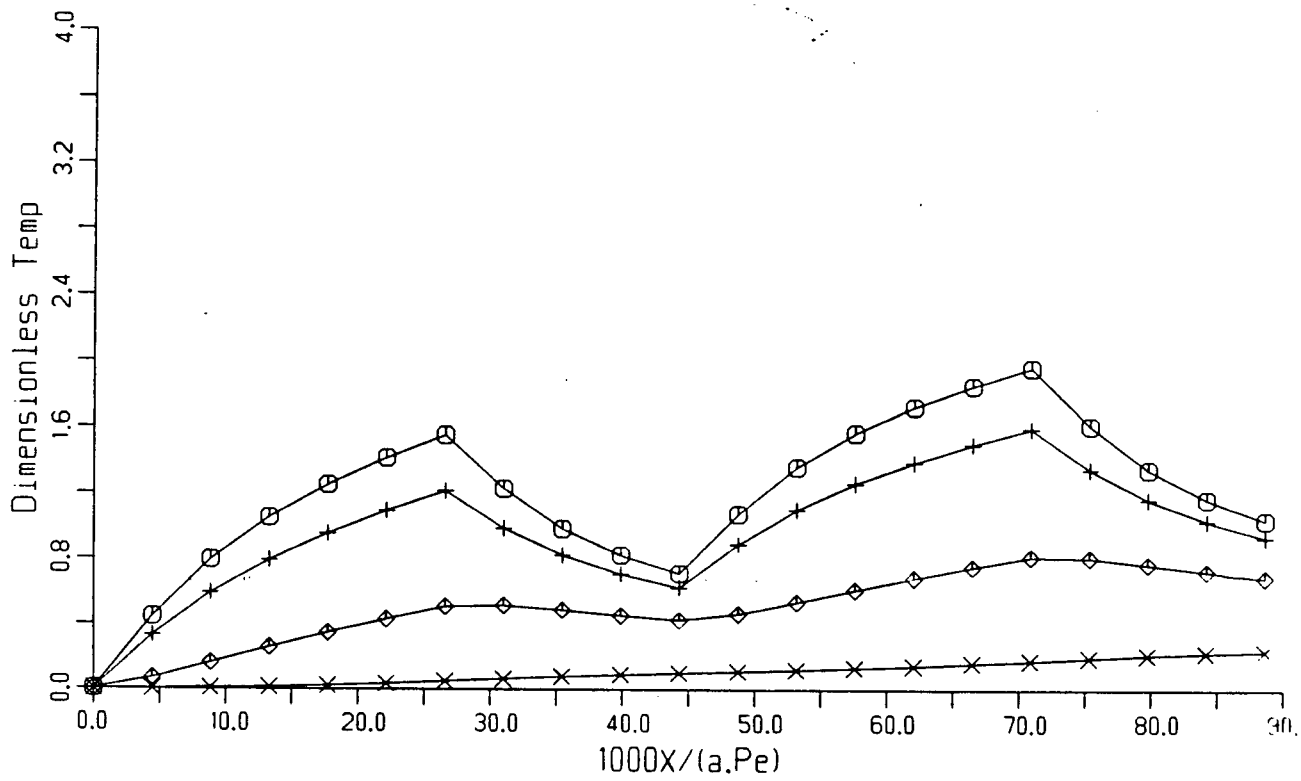

FIG. 4.8. Dimensionless temperature inside the tube at radial co-ordinate r=4/5 versus dimensionless axial distance 1000x=1000X/a·Pe for a spot-welded tube with 2 spots occupying 60% of its length, spot angle 45°.

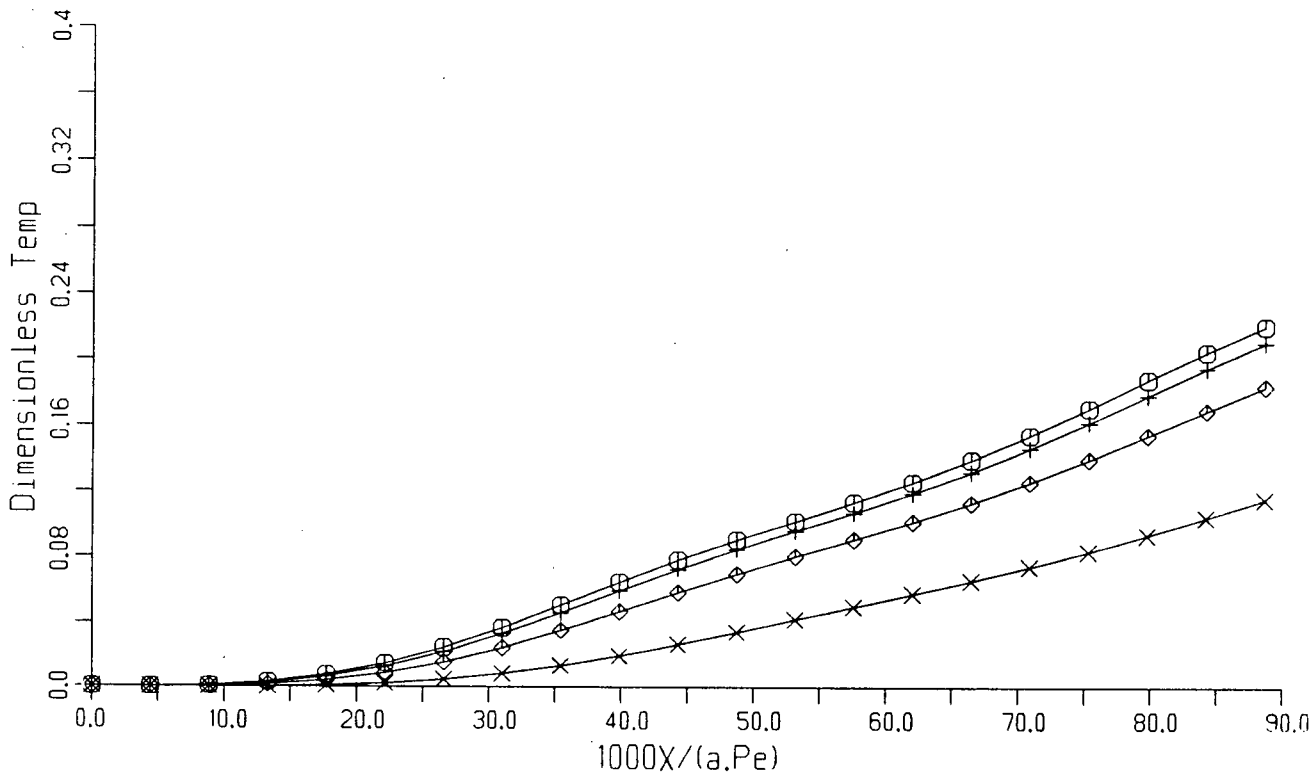

FIG. 4.9. Dimensionless temperature inside the tube at radial co-ordinate r=1/5 versus dimensionless axial distance 1000x = 1000X/a·Pe for a spot-welded tube with 2 spots occupying 60% of its length, spot angle 45°.

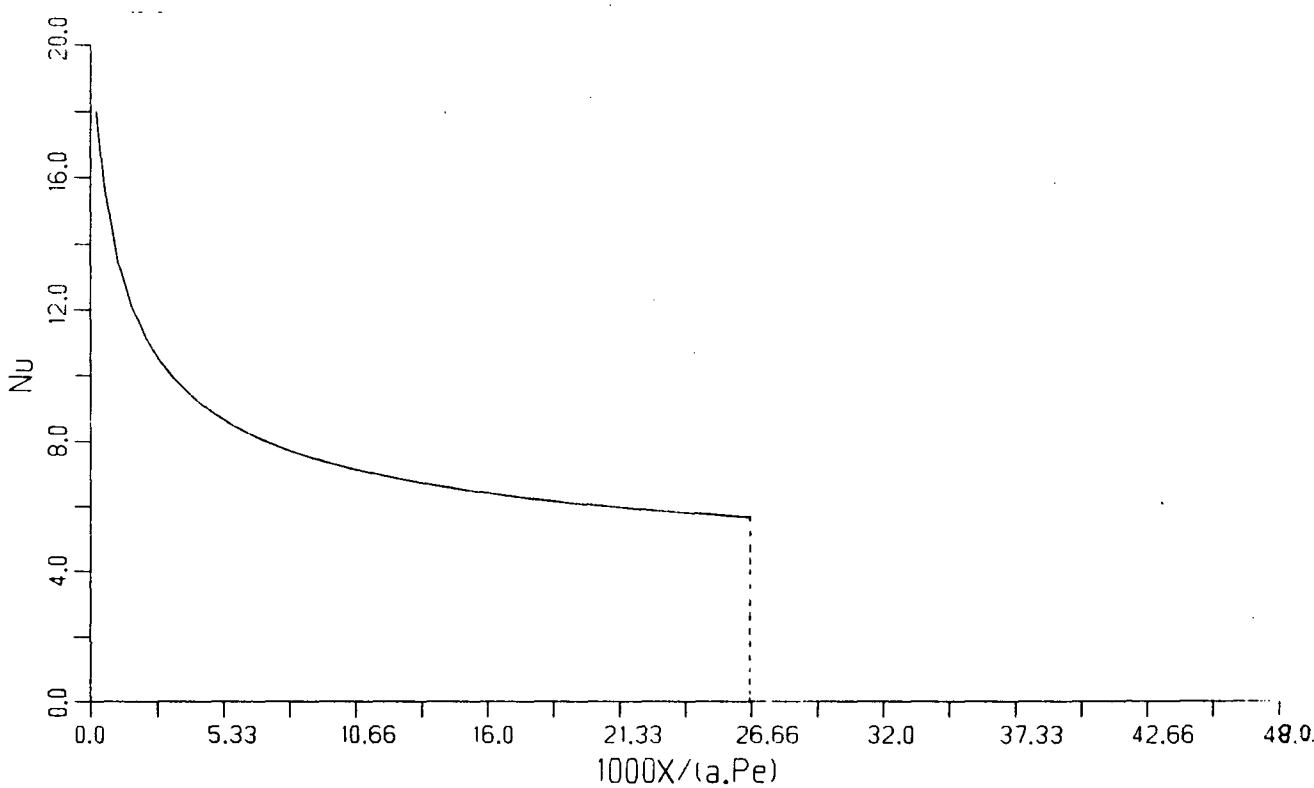

FIG. 4.10(i). Peripheral average Nusselt no. Nu_p versus dimensionless axial distance $1000x = 1000X/a \cdot Pe$: finite difference results for a spot-welded tube with a single spot occupying 60% of its length, spot angle 45°.

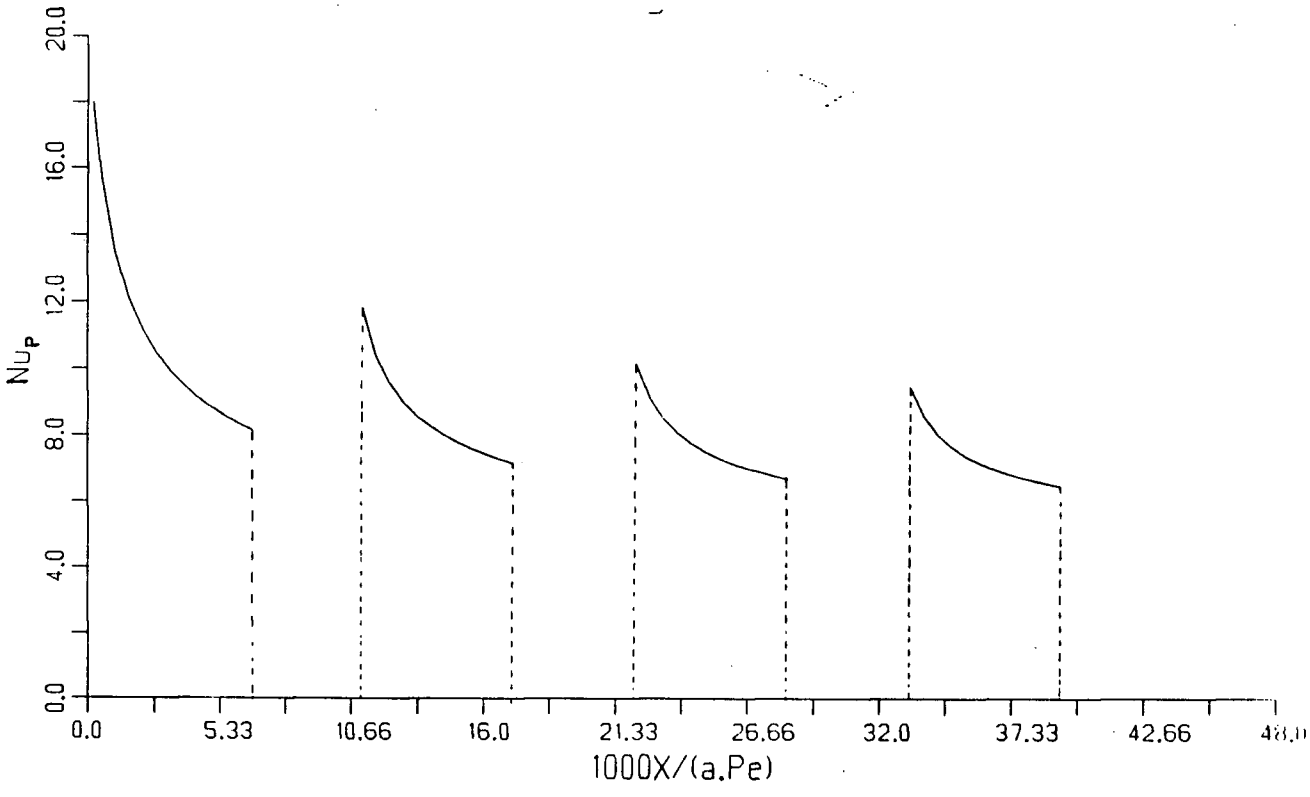

FIG. 4.10(ii). Peripheral average Nusselt Nu_p versus dimensionless axial distance $1000x=1000X/a \cdot Pe$: finite difference results for a spot-welded tube with 4 spots occupying 60% of its length, spot angle 45°.

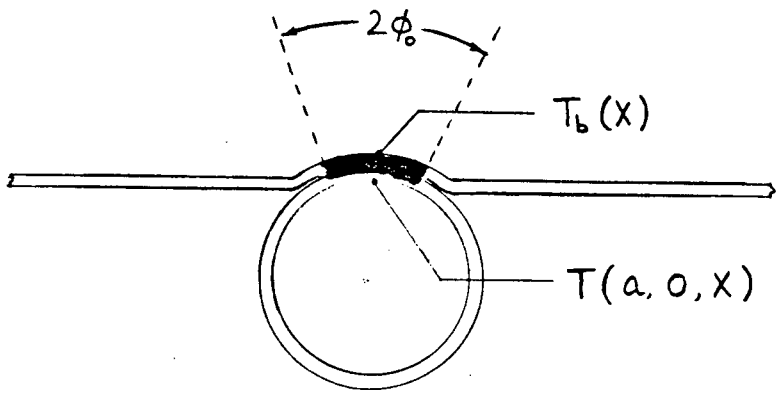

FIG 5.1 Bond temperature $T_b(X)$ approximated by T(a,0,X)

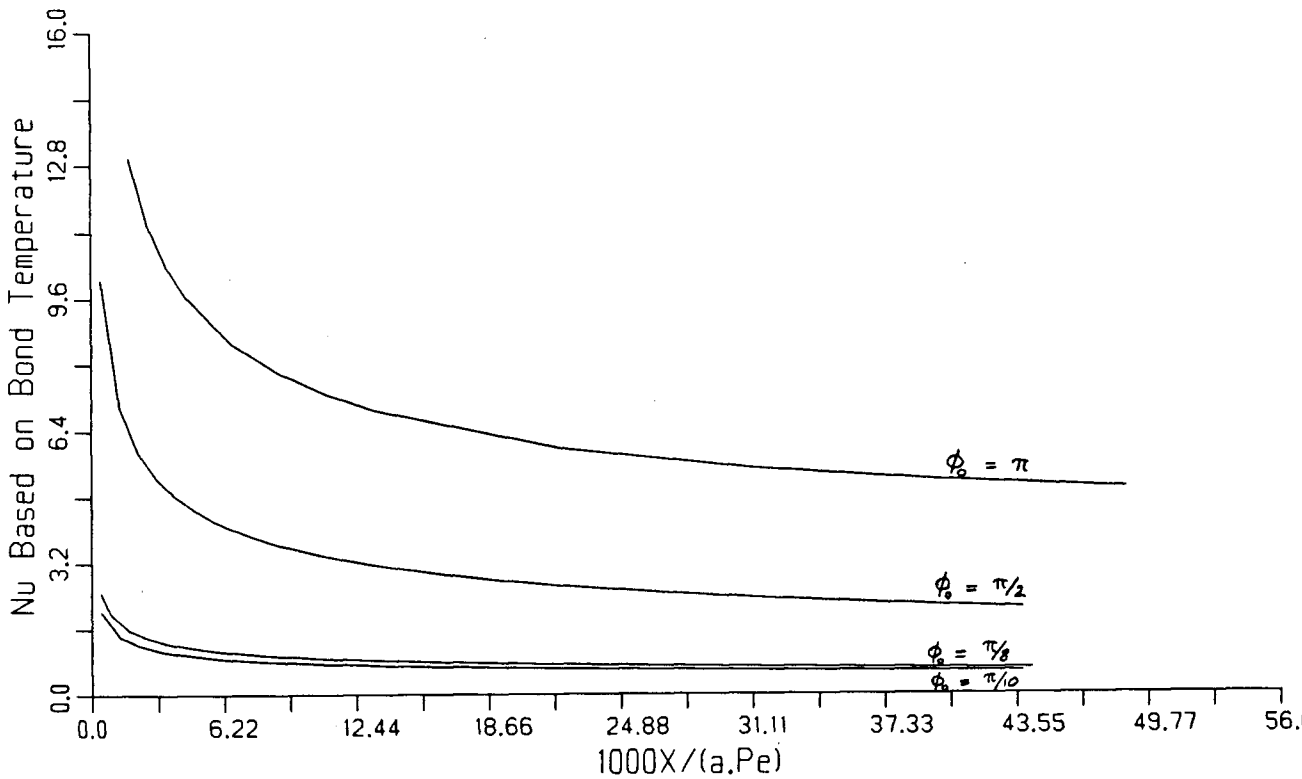

FIG. 5.2. Nusselt no. based on bond temperature Nu_b versus dimensionless axial distance $1000x=1000X/a\cdot Pe$ for a continuously welded tube of various half-spot angles ϕ_o

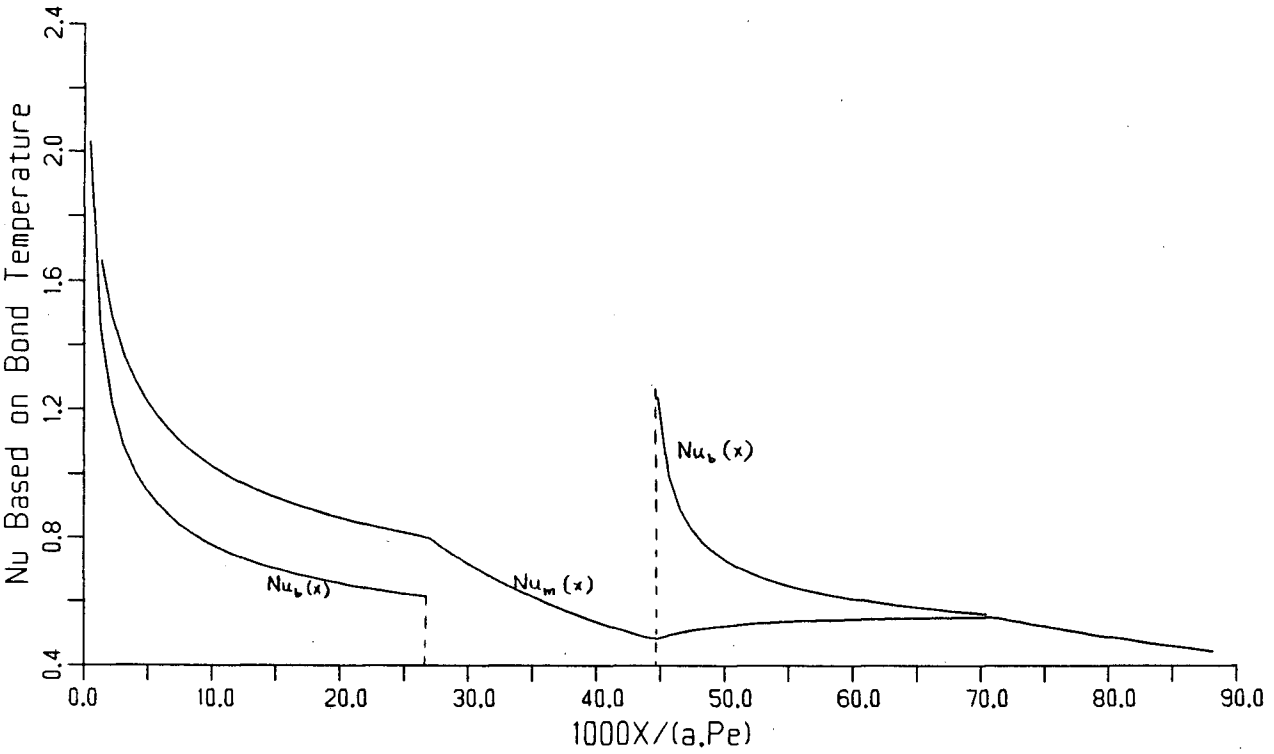

FIG. 5.3. Nusselt no. based on bond temperature Nu_b and mean Nusselt no. based on bond temperature Nu_{bm} versus dimensionless axial distance $1000x=1000X/a \cdot Pe$ for a spot-welded tube with 2 spots occupying 60% of its length, spot angle 36°.

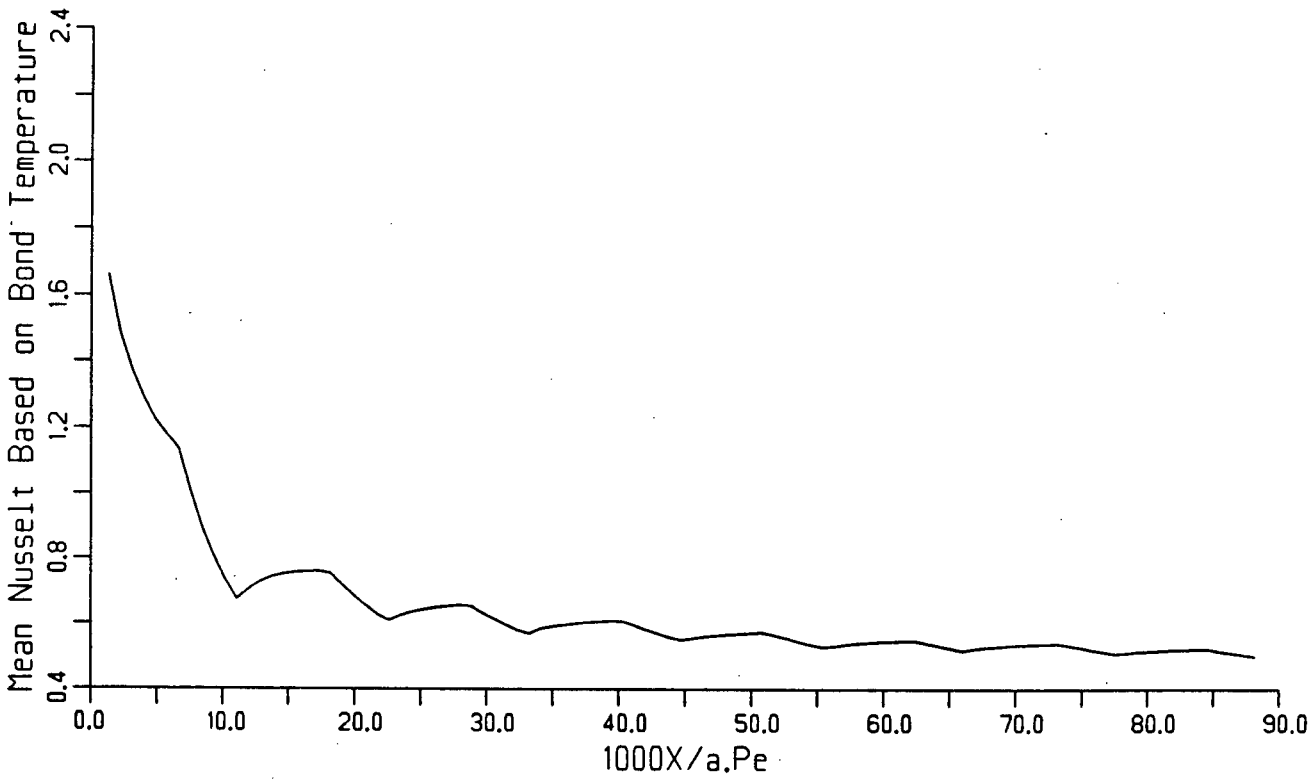

FIG. 5.4. Mean Nusselt no. based on bond temperature Nu_{bm} versus dimensionless axial distance 1000x=1000X/a·Pe for a spot-welded tube with 8 spots occupying 60% of its length, spot angle 36°.

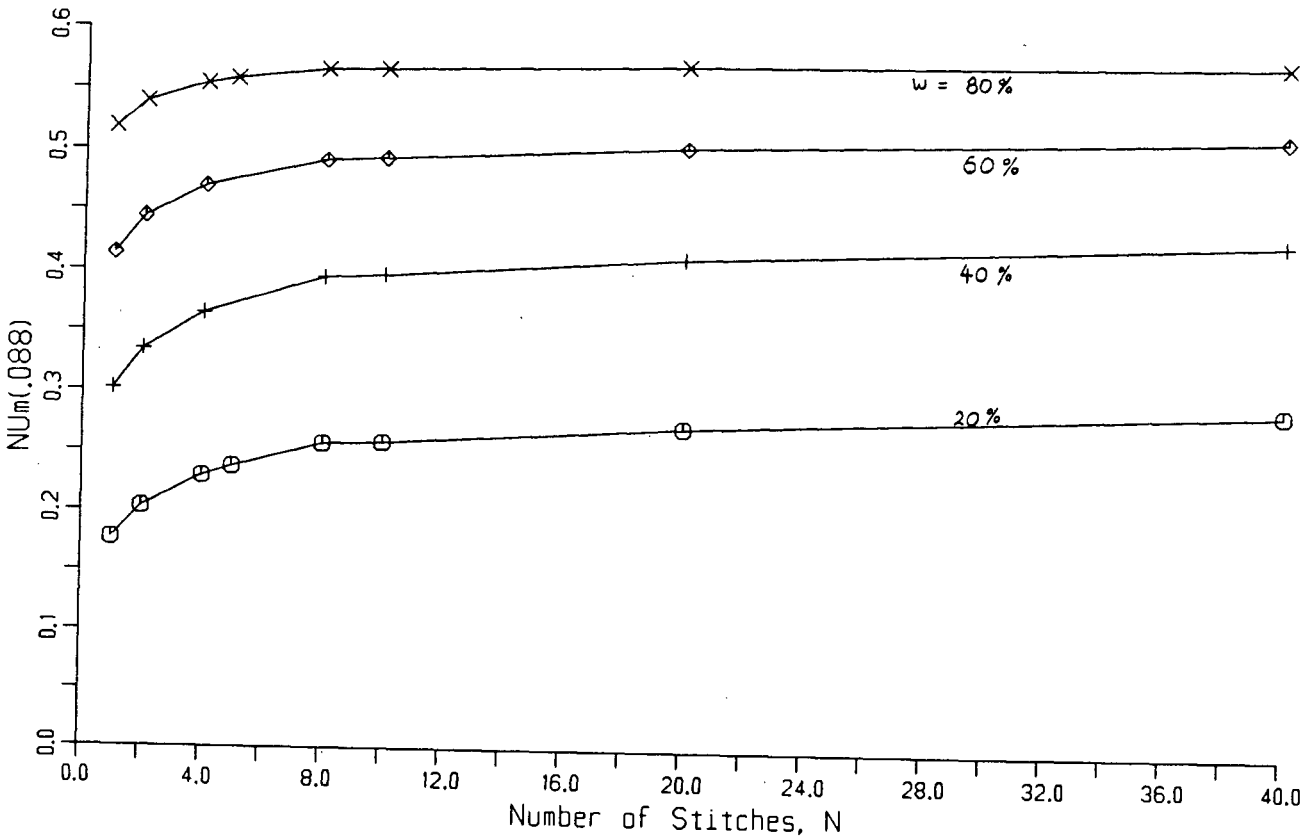

FIG. 5.5. Mean Nusselt no. based on bond temperature Nu_{bm} over a dimensionless tube length of .088 as a function of spot configurations for a spot-welded tube with spot angle of 36°.

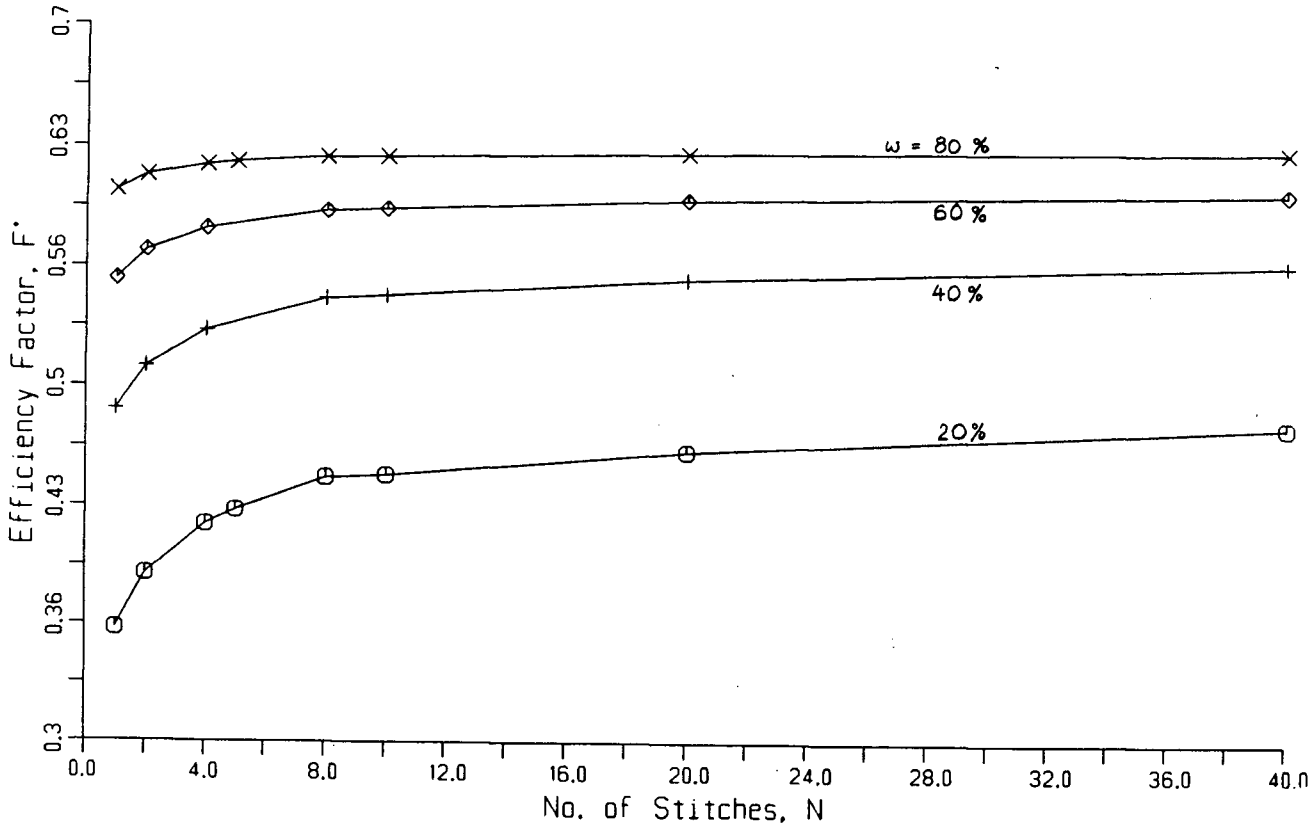

FIG. 5.6. Efficiency Factor F' as a function of spot configurations for a collector with distance W between its spot-welded tubes of .15m and spot angle of 36°.

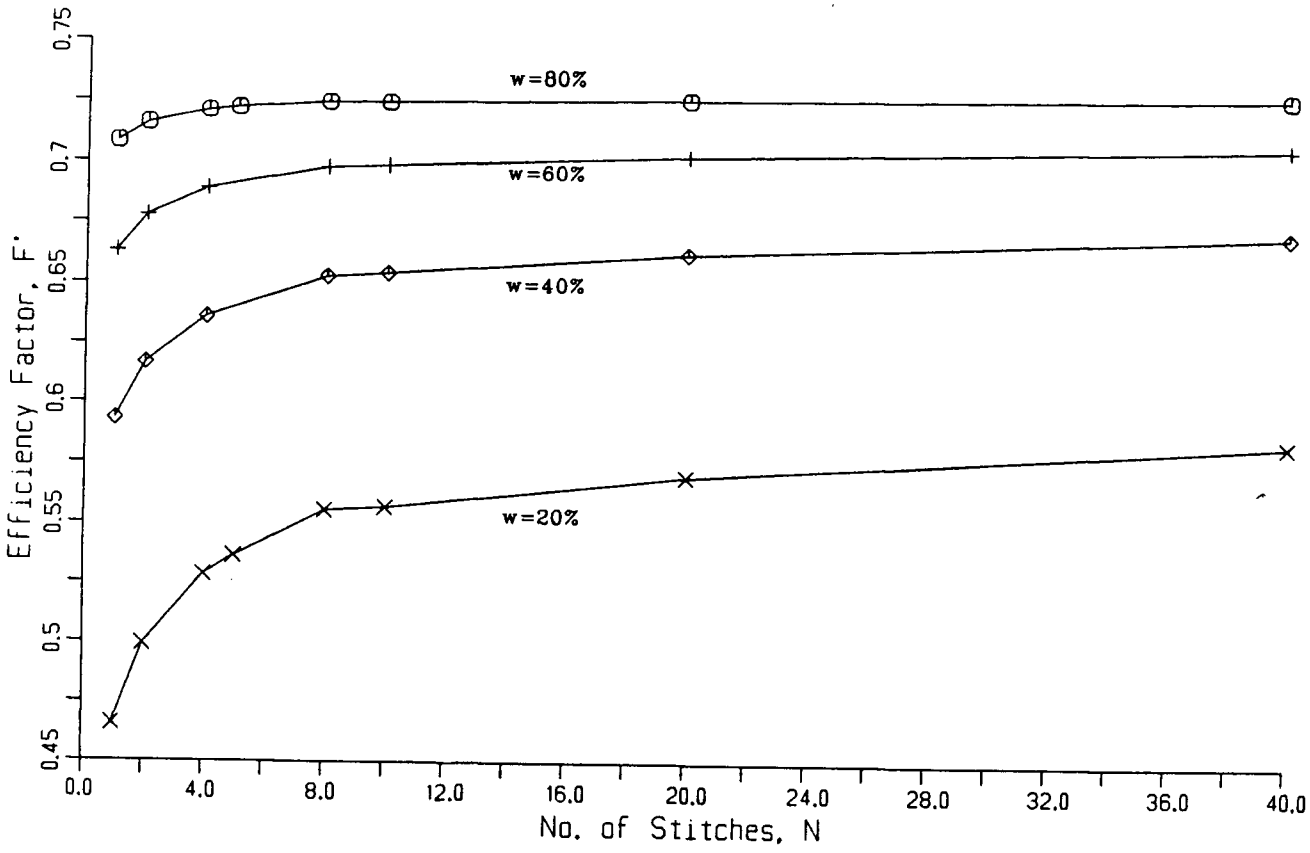

FIG. 6.1. Efficiency Factor F' as a function of spot configurations for a collector with distance W between its spot-welded tubes of .1m and spot angle of 36°.

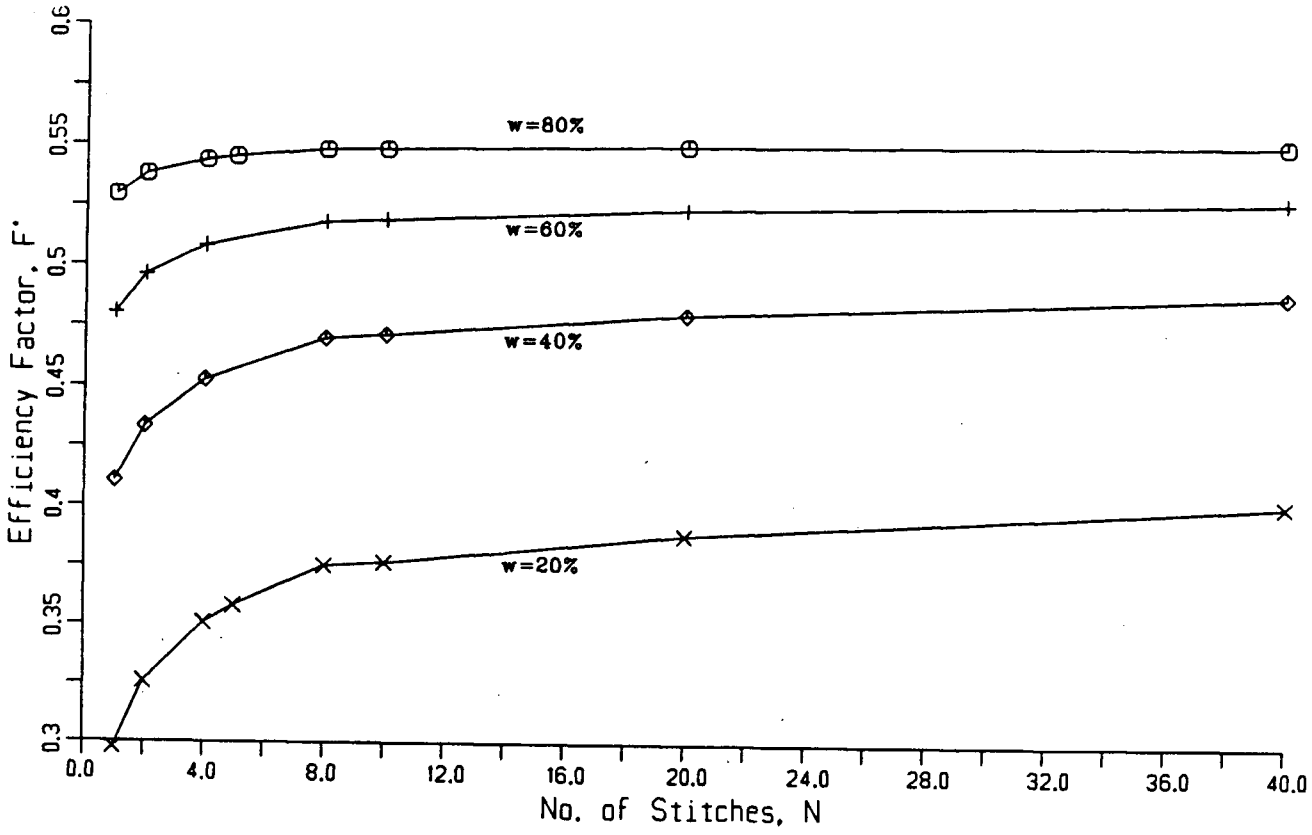

FIG. 6.2. Efficiency Factor F' as a function of spot configurations for a collector with distance W between its spot-welded tubes of .2m and spot angle of 36°.

APPENDIX A

Specifications of a Typical Two-cover Solar Collector

Collector Dimensions

Tube inner radius, a = 4.5×10^{-3}m

Cross sectional area of tube, A = 6.36×10^{-5}m^2

Tube length, L = 2m

Collector area = 2m x 1m

Absorber plate thickness, δ = 2.54×10^{-4}m

Tube wall thickness, γ = 5×10^{-4}m

Distance between tubes, W = 0.15m

Fluid Properties (50°C)

Specific heat capacity, c_p = 4.174 kJ/kg°C

Thermal conductivity, k = 0.644 W/m°C

Thermal diffusivity, α = 1.561×10^{-7} m^2/s

Density, ρ = 988.8 kg/m^3

Dynamic viscosity, μ = 5.62×10^{-4}kg/ms

Kinematic viscosity, ν = 5.68×10^{-7}m^2/s

Prandtl no., Pr = ν/α = 3.64

Other Parameters

Coolant flow rate per tube, $\dot{m}$ = 5.55×10^{-3}kg/s

Mean flow speed, $\bar{u} = \dot{m}/\rho A$ = 0.088 m/s

Reynolds no. of coolant flow, Re = 1390

Peclet's no. of coolant flow, Pe = RePr = 5060

Thermal conductivity of plate and tube material(copper),

$k_s = k_w = 385$ W/m°C

Collector overall heat transfer coefficient,

$U_L = 4$ W/m²°C

APPENDIX B

Effect of Fluid Axial Conduction

Fluid axial conduction has not been accounted for in the analysis as its representative term $\partial^2 t/\partial x^2$ was omitted from the energy equation at the beginning. This term is important only when Peclet No. is small(Pe<100). In any case, its effect is obvious only at a short distance from the step change in thermal boundary condition, as can be seen from the results of Hsu[21] for the uniformly heated tube. Taking axial conduction into account, the Nusselt no. Nu(x) obtained for $x<10^{-2}$ is lower than that obtained with axial conduction neglected (which corresponds to the case where $Pe=\infty$), and this discrepancy increases as x decreases.

For $Pe\simeq 5000$, an axial distance X of one tube radius corresponds to

$$x = X/a\cdot Pe \simeq 1/5000 = 2\times 10^{-4}.$$

Since the superposed solution, i.e. Nu(x), for the "thin" spot-welded tube makes use, along the entire flow length, of values corresponding to very small x, the effect of fluid axial conduction has caused concerns, especially when the spot length is of the same order of magnitude as the radius. However, the error can be shown to be insignificant.

Let Nu(x) and $Nu_\infty(x)$ represent the Nusselt no. distribution of a continuously welded tube with $Pe<\infty$ and $Pe=\infty$ respectively, and $Nu^S(x)$ and $Nu^S_\infty(x)$ represent the

Nusselt no. distribution of a spot-welded tube with Pe<∞ and Pe=∞ respectively. Also let

$$1/Nu(x) - 1/Nu_{\infty}(x) = \epsilon(x) \ ,$$

then
$$\begin{aligned} 1/Nu^{S}(x) &= 1/Nu(x) - H(x-x_1)/Nu(x-x_1) + \\ &\quad H(x-x_1-x_s)/Nu(x-x_1-x_s) - .... \\ &= 1/Nu_{\infty}(x) + \epsilon(x) \\ &\quad - H(x-x_1)[1/Nu_{\infty}(x-x_1) + \epsilon(x-x_1)] + \\ &\quad H(x-x_1-x_s)[1/Nu(x-x_1-x_s) + \epsilon(x-x_1-x_s)] - ... \\ &= 1/Nu^{S}_{\infty}(x) + \epsilon(x) - \epsilon(x-x_1)H(x-x_1) + \\ &\quad \epsilon(x-x_1-x_s)H(x-x_1-x_s) - .... \end{aligned}$$

Thus, the error $1/Nu^{S}(x) - 1/Nu^{S}_{\infty}(x)$

$$= \epsilon(x) - \epsilon(x-x_1)H(x-x_1) + \epsilon(x-x_1-x_s)H(x-x_1-x_s) - ....$$

When x is small, $\epsilon(x)$ is small since both $Nu^{S}(x)$ and $Nu^{S}_{\infty}(x)$ are large. When x is large ($x>10^{-2}$), Nu^{S} approaches Nu^{S}_{∞} and $\epsilon(x)$ approaches zero. Furthermore, the individual terms in the error series have a cancellation effect on each other, so that there is no accumulating error involved in the superposed solution.

In conclusion, the discrepancy between Nu^{S} and $Nu^{S}_{\infty}(x)$ exists not only at small x but along the whole tube length. However, the large Peclet no. of 5060 in the present case renders that discrepancy negligible.

APPENDIX C

Expression of $S(\bar{\nabla}\bar{V})$ and Φ in Cartesian Coordinates

The stress tensor :

$$S = \begin{pmatrix} s_{xx} & s_{xy} & s_{xz} \\ s_{yx} & s_{yy} & s_{yz} \\ s_{zx} & s_{zy} & s_{zz} \end{pmatrix},$$

where s_{yx} denotes the stress acting along the x direction on the surface normal to the y-axis.

The Velocity Deformation Tensor :

$$\bar{\nabla}\bar{V} = \begin{pmatrix} \partial u/\partial x & \partial u/\partial y & \partial u/\partial z \\ \partial v/\partial x & \partial v/\partial y & \partial v/\partial z \\ \partial w/\partial x & \partial w/\partial y & \partial w/\partial z \end{pmatrix},$$

where u, v, w are the x-, y-, z-component, respectively, of the velocity $\bar{V}$.

The Complete Contraction :

$$
\begin{aligned}
S(\,\bar{\nabla}\,\bar{V}\,) = \quad & + s_{xx}\,\partial u/\partial x + s_{yx}\,\partial u/\partial y + s_{zx}\,\partial u/\partial z \\
& + s_{xy}\,\partial v/\partial x + s_{yy}\,\partial v/\partial y + s_{zy}\,\partial v/\partial z \\
& + s_{xz}\,\partial w/\partial x + s_{yz}\,\partial w/\partial y + s_{zz}\,\partial w/\partial z .
\end{aligned}
$$

The Dissipation Function :

$$
\begin{aligned}
\Phi = \quad & 2\,[(\partial u/\partial x)^2 + (\partial v/\partial y)^2 + (\partial w/\partial z)^2\,] \\
& - (2/3)(\,\bar{\nabla}\cdot\bar{V}\,)^2 + (\,\partial u/\partial y + \partial v/\partial x\,)^2 \\
& + (\,\partial v/\partial z + \partial w/\partial y\,)^2 + (\,\partial w/\partial x + \partial u/\partial z\,)^2 .
\end{aligned}
$$